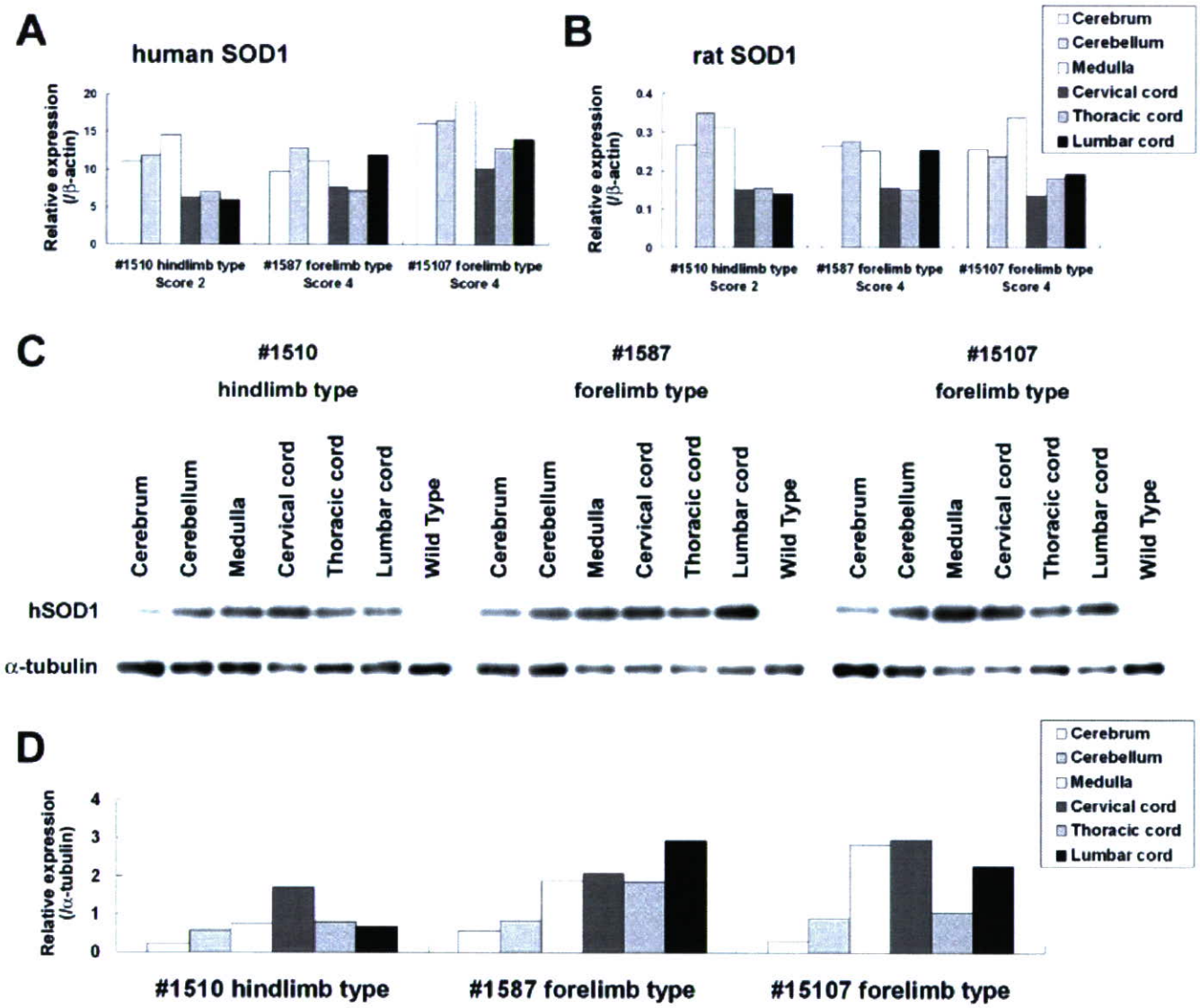

Fig. 6. The expression of mutant hSOD1 mRNA and protein in the cerebral cortex, cerebellum, medulla, and spinal cord (cervical, thoracic, and lumbar) of forelimb- and hindlimb-type rats. **A,B:** The amounts of human (A) and endogenous rat (B) SOD1 mRNA normalized to those of *β-actin* were quantified by real time RT-PCR analysis. **C,D:** Western blot analysis of the mutant hSOD1 protein was carried out in the same rats. Quantitative analysis was carried out with a Scion Image. The amounts of proteins were normalized to those of α-tubulin (D).

hindlimb-type rats by real time RT-PCR and Western blot analysis. However, at least at the stages after the apparent onset of muscle weakness, neither forelimb-type (#1587, Score 4 and #15107, Score 4) nor hindlimb-type rats (#1510, Score 2) necessarily expressed larger amounts of the mutant hSOD1 (G93A) transgene in the cervical cord or in the lumbar cord, respectively, at the mRNA and the protein level (Fig. 6). We also investigated the expression of endogenous rat SOD1 mRNA in the same rats by REAL TIME RT-PCR (Fig. 6B). Distribution of endogenous rat SOD1 mRNA expressed in each segment of the spinal cord showed almost the same pattern as that of mutant hSOD1 mRNA. The expression of endogenous rat SOD1 mRNA was lower than that of mutant hSOD1 mRNA. Thus, we could not detect any definite correlation between the hSOD1 (G93A) transgene local expression profile in the spinal cord and the phenotypes of G93A rats for either the forelimb-type or the hindlimb-type rats (Fig. 6).

Reduction in the Number of Spinal Cord Motor Neurons at Different Disease Stages

We examined histo-pathological changes in the spinal cords of the transgenic rats in comparison with those

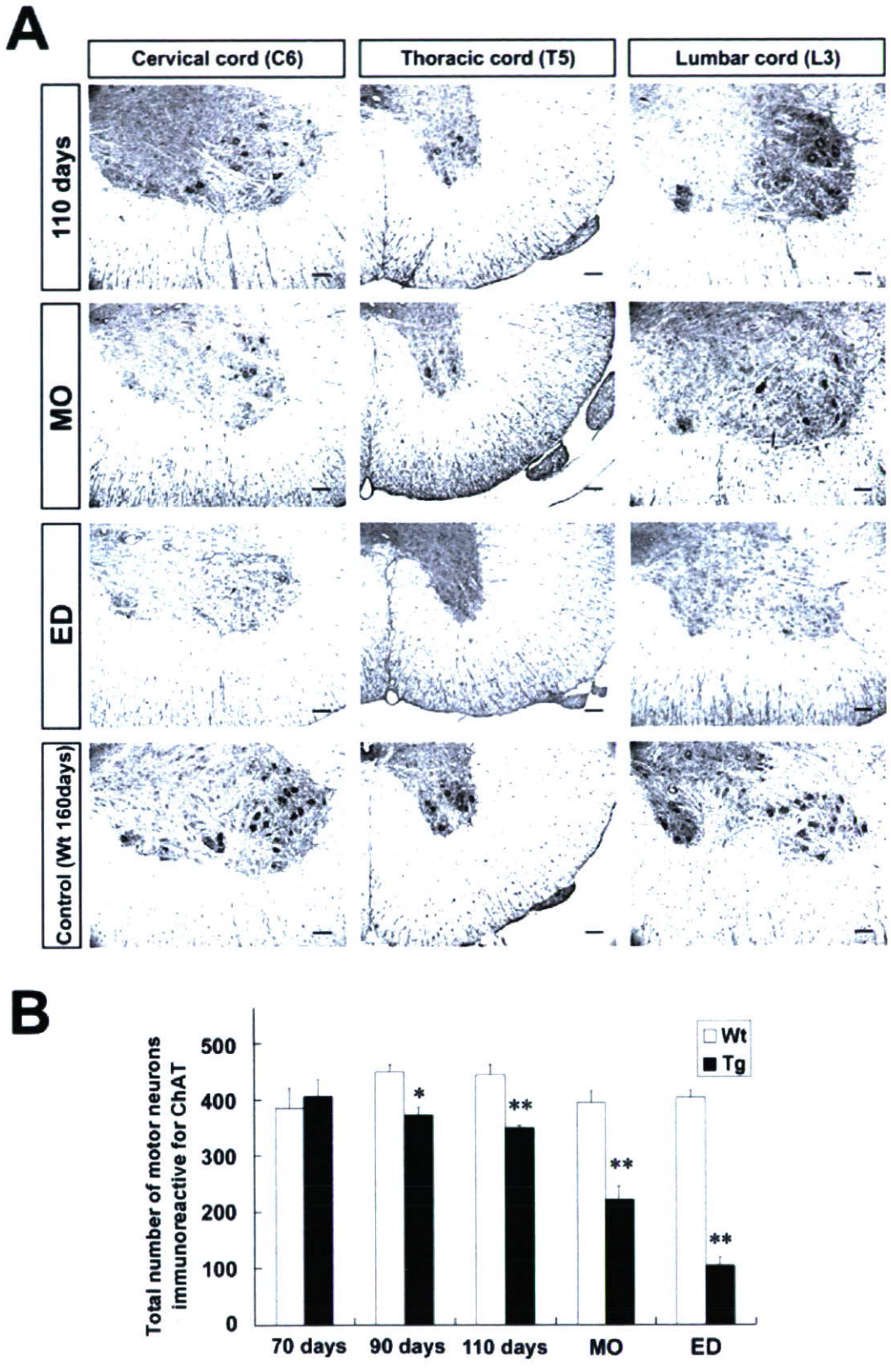

Fig. 7. The loss of motor neurons in the spinal cord of hSOD1 (G93A) transgenic rats at different stages. **A:** Immunohistochemical analysis of the spinal cord of transgenic rats. Transverse sections of the cervical (C6), thoracic (T5), and lumbar (L3) spinal cord of the transgenic rats and their wild-type littermates were stained with an anti-ChAT antibody to label viable motor neurons at the indicated stages (Scale bars = 100 μm). **B:** The number of ChAT immunoreactive motor neurons was counted and is shown in the histograms as the total number of motor neurons in the C6, T5, and L3 segments. This number began to decrease in the transgenic rats at 90 days of age, rapidly declined after 110 days of age, and fell to about 50% and 25% of wild-type rats at the muscle weakness onset (MO, around 125 days) and at end-stage disease (ED, around 140 days), respectively. Bars = means ± SEM ($n = 3$ for each genotype). $^{*}P < 0.05$. $^{**}P < 0.01$; two-tailed unpaired Student's t-test.

of their wild-type littermates at 70, 90, and 110 days of age, when the transgenic rats scored <70° in the inclined plane test (muscle weakness onset), and failed the righting reflex. To quantify the number of spinal motor neurons, we stained spinal cord sections of both groups with an anti-ChAT antibody.

As shown in Figure 7A, the numbers of ChAT immunoreactive motor neurons in the cervical (C6), thoracic (T5), and lumbar (L3) segments of the spinal cord decreased with disease progression. Quantitative analysis of the residual motor neurons showed that the total number of motor neurons in the transgenic rats began to decrease at 90 days of age, rapidly declined after 110 days of age, and fell to about 50% and 25% of the numbers in age-matched wild-type littermates at the time the score was <70° in the inclined plane test (muscle weakness onset) and of righting reflex failure, respectively (Fig. 7B).

TABLE VI. Adequacy of Evaluation Methods in Regard to Practical Use*

	Body weight	Inclined plane	Cage activity	SCANET	Motor score
Objectivity	A	B	A	A	B
Sensitivity	A	B	C	(A)	-
Specificity	C	B	C	C	A
Motivation independence	A	B	B	D	B
Skill requirements	A	B	A	A	B
Cost of apparatus	B	B	D	D	A

*A, more appropriate; B, appropriate; C, less appropriate; D, inappropriate.

DISCUSSION

Factors Underlying the Variability in Phenotypes of hSOD1 (G93A) Transgenic Rats

In previous studies of this G93A rat, only the hindlimb-type has been described, and the variety of phenotypes and variable clinical courses have not yet been mentioned (Nagai et al., 2001). Recently, however, another line of G93A rats backcrossed onto a Wistar background ($SOD1^{G93A/HWr}$ rats) was reported to present two phenotypes, including forelimb-type, and a large inter-litter variability in disease onset (Storkebaum et al., 2005). In the same way, commonly used FALS model mice harboring hSOD1 (G93A) gene have been reported to have clinical variability to some extent, and some of them dominantly show forelimb paralysis (Gurney et al., 1994). In this study, we recognized various clinical types, including forelimb-, hindlimb-, and general-type and established quantitative methods to evaluate disease progression that can be applied to any of the clinical types of this ALS model. We have also shown the variability in disease progression to depend on clinical types, that is, disease progression after the onset was faster in forelimb-type than in hindlimb-type rats. This difference may be due to the aggressiveness of the disease per se because we evaluated the time point of "death" (end-stage disease) according to righting reflex failure (Howland et al., 2002) to exclude the influence of feeding problems (bulbar region) and respiratory failure (level C2–C4).

These findings give rise to the next question; why is this variety of phenotypes and variability in the clinical course observed in the same transgenic line? There are at least three possible explanations. One is that the variation is due to the heterogeneous genetic background of the Sprague-Dawley (SD) rat (i.e., the strain used to generate this transgenic line), which might have led to different phenotypes. This idea is supported by the fact that the SD strain shows a large inter-individual disease variability in other models of neurodegenerative disorders, such as Huntington's disease (Ouary et al., 2000). Similar phenotypic variability takes place in human FALS carrying the same mutations in hSOD1 gene (Abe et al., 1996; Watanabe et al., 1997; Kato et al., 2001), which could be explained by heterogeneous genetic backgrounds. Thus, the present transgenic ALS model rats may be highly useful to understand the mechanisms of bulbar onset, arm onset, or leg onset that are seen in human disease. There may be modifier genes of these phenotypes, which should be identified in the future study.

The second is that there is variability in the expression of the mutant hSOD1 protein. The transcriptional regulation of this exogenous gene could be affected by one or more unknown factors, such as epigenetic regulation, and may not be expressed uniformly throughout the spinal cord of each animal. Therefore, some rats might express mutant proteins more in the cervical spinal cord and others might express more in the lumber cord, possibly resulting in the forelimb type and hindlimb type, respectively. However, we found no definite correlation between local expression levels of the mutant hSOD1 mRNA/protein in the spinal cord and the phenotypes of these animals, using real time RT-PCR and western blot analysis after the onset of muscle weakness, when the clinical type of the transgenic rats could be defined (Fig. 6). Moreover, the pathological analysis showed no correlation between the number of residual motor neurons in each segment and the phenotypes of end-stage animals. However, because >50% of spinal motor neurons have already degenerated at the stage of muscle weakness onset, whether local expression of the mutant hSOD1 gene and segmental loss of motor neurons correlate with the clinical types of G93A rats should be further investigated by analyzing younger animals at a stage when motor neuron loss has not progressed as much.

The third explanation involves a structural property of the mutant hSOD1 (G93A) protein itself. It is now thought that mutations in the hSOD1 gene may alter the 3-D conformation of the enzyme and, in turn, result in the SOD1 protein acquiring toxic properties that cause ALS (Deng et al., 1993; Hand and Rouleau 2002). For instance, the hSOD1 (G93A) mutant protein has been reported to be susceptible to nonnative protein–protein interactions because of its mutation site and unfolded structure (Shipp et al., 2003; Furukawa and

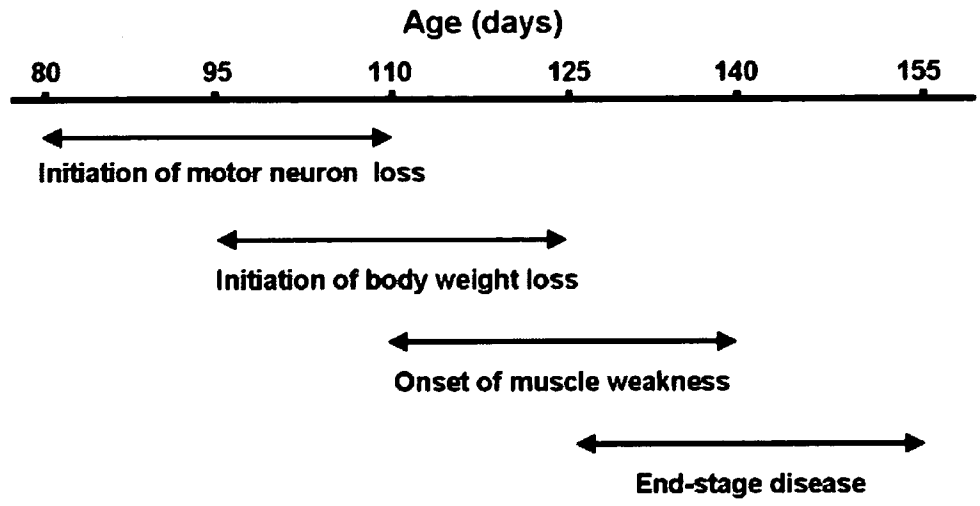

Fig. 8. Four stages of disease progression in hSOD1 (G93A) transgenic rats. The disease progression can be classified into four stages as shown. The range for each stage is about 1 month and overlaps approximately 2 weeks with the next stage.

O'Halloran, 2005), suggesting that the G93A mutation might accelerate the formation of SOD1 protein aggregates, which may ultimately sequester heat-shock proteins and molecular chaperones, disturb axonal transport or protein degradation machineries, including the ubiquitin-proteasome system (Borchelt et al., 1998; Bruening et al., 1999; Williamson and Cleveland 1999; Okado-Matsumoto and Fridovich 2002; Urushitani et al., 2002). Curiously, the mutated hSOD1 (G93A) protein is more susceptible to degradation by the ubiquitin-proteasome system and has a shorter half-life than other mutants (Fujiwara et al., 2005), suggesting that it may cause more unstable toxic aggregates in the spinal cord than other mutations. The degradation rate is also affected by environmental factors unique to each animal, such as the progressive decline of proteasome function with age (Keller et al., 2000), and these factors could contribute to the variability of the clinical course of G93A rats.

Taking all these findings into consideration, the mutated hSOD1 (G93A) protein may gain properties that are responsible for a variety of phenotypes and variability in the clinical course of the affected animals.

Characteristics of Different Methods for Assessing hSOD1 (G93A) Transgenic Rats

The ideal measure is not influenced by the judgment of the observer, sensitive to small abnormalities, specific to detect pathologic events that are related to pathogenesis of the ALS-like disease, not influenced by the motivational factors of rats, minimal in the requirements for skill in the observer, and inexpensive to carry out. We assessed each evaluation method by the categories in regard to practical use as shown in the Table 6.

The initiation of body weight loss seems to be an excellent marker to detect the onset and should be highly recommended. Muscle volume might have already started to decrease, even in the period of continuous weight gain, as reported for hSOD1 (G93A) transgenic mice (Brooks et al., 2004). As a result, it could detect an abnormality relatively earlier than subjective onset. The inclined plane test is considered to be the least defective method of all. It could objectively and specifically detect the decline in the muscle strength of these ALS model rats as a muscle weakness onset almost at the same time of the subjective onset. The cage activity measurement and SCANET require very expensive apparatus, and are limited by the availability of funds and space for making the measurements. Although SCANET test was most sensitive among these measures, it seems inappropriate for the statistical analysis, and does not add any more information than that obtained through simple observation of the rats because the performances of the rats might be severely affected by the extent of their motivation to explore. Motor score can specifically assess disease progression of each clinical type and is valuable in keeping the experimental costs at a minimum.

Correlation Between the Loss of Spinal Motor Neurons and Disease Stages

This study clearly shows the variable clinical course of G93A rats. According to our behavioral and histological analyses, we can divide the disease course of this transgenic model into four stages, whose durations have a range of about 1 month, as shown in Figure 8. Furthermore, we have established the pathological validity of the performance deficits detected by each measure of disease progression. "Initiation of motor neuron loss" was defined as a statistically significant decrease in the number of spinal motor neurons, which was found at around 90 days of age, but not 70 days of age (Fig. 7B). This coincides with, and seems to be sensitively detected by the marked difference in SCANET scores that begins at around 90 days of age (Fig. 3D–F). The "initiation of body weight loss" was usually detected at around 110 days of age as the peak body weight (pre-symptomatic onset, 113.6 ± 4.8 days of age, range = 103–124, Table IV). This stage coincides with the initiation of a rapid decline in the number of motor neurons at around 110 days of age (Fig. 7B). "Onset of muscle weakness" was detected at around 125 days of age, as assessed by the

inclined plane test (muscle weakness onset, 125.2 ± 7.4 days of age, range = 110–144, Table IV). This coincides with the number of spinal motor neurons in the transgenic rats being reduced to about 50% of the number in wild-type rats (Fig. 7B). We presume that transgenic rats do not present obvious muscle weakness until the number of motor neurons has been reduced to approximately half the number found in the healthy state. "End-stage disease" as defined by righting reflex failure was recorded at around 140 days of age (137.8 ± 7.1 days of age, range = 122–155, Table IV). At this stage, the affected rats had only about 25% of the spinal motor neurons of age- and gender-matched wild-type rats (Fig. 7B), and showed a generalized loss of motor activity. Thus, our findings allow us to estimate the extent of spinal motor neuron loss by evaluating the disease stage with the measures described in this study.

In summary, we have described the variable phenotypes of mutant hSOD1 (G93A) transgenic rats and established an evaluation system applicable to all clinical types of these rats. Disease stages defined by this evaluation system correlated well pathologically with the reduction of motor neurons. Our evaluation system of this animal model should be a valuable tool for future preclinical experiments aimed at developing novel treatments for ALS.

ACKNOWLEDGMENTS

We thank Dr. H.-N. Dai of the Department of Neuroscience, Georgetown University School of Medicine for technical advice and valuable discussions, and Dr. T. Yoshizaki and Miss K. Kaneko for participating in the assessment of transgenic rats with the Motor score. This work was supported by grants from CREST, Japan Society for the Promotion of Science to H.O., a Research Grant on Measures for Intractable Diseases from the Japanese Ministry of Health, Labour and Welfare to H.O., M.A., G.S. and Y.I., and a Grant-in-Aid for the 21st century COE program to Keio University from the Japanese Ministry of Education, Culture, Sports, Science and Technology.

REFERENCES

Abe K, Aoki M, Ikeda M, Watanabe M, Hirai S, Itoyama Y. 1996. Clinical characteristics of familial amyotrophic lateral sclerosis with Cu/Zn superoxide dismutase gene mutations. J Neurol Sci 136:108–116.

Azzouz M, Ralph GS, Storkebaum E, Walmsley LE, Mitrophanous KA, Kingsman SM, Carmeliet P, Mazarakis ND. 2004. VEGF delivery with retrogradely transported lentivector prolongs survival in a mouse ALS model. Nature 429:413–417.

Barneoud P, Lolivier J, Sanger DJ, Scatton B, Moser P. 1997. Quantitative motor assessment in FALS mice: a longitudinal study. Neuroreport 8:2861–2865.

Borchelt DR, Wong PC, Becher MW, Pardo CA, Lee MK, Xu ZS, Thinakaran G, Jenkins NA, Copeland NG, Sisodia SS, Cleveland DW, Price DL, Hoffman PN. 1998. Axonal transport of mutant superoxide dismutase 1 and focal axonal abnormalities in the proximal axons of transgenic mice. Neurobiol Dis 5:27–35.

Brooks KJ, Hill MD, Hockings PD, Reid DG. 2004. MRI detects early hindlimb muscle atrophy in Gly93Ala superoxide dismutase-1 (G93A SOD1) transgenic mice, an animal model of familial amyotrophic lateral sclerosis. NMR Biomed 17:28–32.

Brown RH Jr. 1995. Amyotrophic lateral sclerosis: recent insights from genetics and transgenic mice. Cell 80:687–692.

Bruening W, Roy J, Giasson B, Figlewicz DA, Mushynski WE, Durham HD. 1999. Up-regulation of protein chaperones preserves viability of cells expressing toxic Cu/Zn-superoxide dismutase mutants associated with amyotrophic lateral sclerosis. J Neurochem 72:693–699.

Chiu AY, Zhai P, Dal Canto MC, Peters TM, Kwon YW, Prattis SM, Gurney ME. 1995. Age-dependent penetrance of disease in a transgenic mouse model of familial amyotrophic lateral sclerosis. Mol Cell Neurosci 6:349–362.

de Belleroche J, Orrell R, King A. 1995. Familial amyotrophic lateral sclerosis/motor neurone disease (FALS): a review of current developments. J Med Genet 32:841–847.

Deng HX, Hentati A, Tainer JA, Iqbal Z, Cayabyab A, Hung WY, Getzoff ED, Hu P, Herzfeldt B, Roos RP, Warner C, Deng G, Soriano E, Smyth C, Parge HE, Ahmed A, Roses AD, Hallewell RA, Pericak-Vance MA, Siddique T. 1993. Amyotrophic lateral sclerosis and structural defects in Cu, Zn superoxide dismutase. Science 261:1047–1051.

Fujiwara N, Miyamoto Y, Ogasahara K, Takahashi M, Ikegami T, Takamiya R, Suzuki K, Taniguchi N. 2005. Different immunoreactivity against monoclonal antibodies between wild-type and mutant copper/zinc superoxide dismutase linked to amyotrophic lateral sclerosis. J Biol Chem 280:5061–5070.

Furukawa Y, O'Halloran TV. 2005. Amyotrophic lateral sclerosis mutations have the greatest destabilizing effect on the Apo- and reduced form of SOD1, leading to unfolding and oxidative aggregation. J Biol Chem 280:17266–17274.

Gale K, Kerasidis H, Wrathall JR. 1985. Spinal cord contusion in the rat: behavioral analysis of functional neurologic impairment. Exp Neurol 88:123–134.

Garbuzova-Davis S, Willing AE, Milliken M, Saporta S, Zigova T, Cahill DW, Sanberg PR. 2002. Positive effect of transplantation of hNT neurons (NTera 2/D1 cell-line) in a model of familial amyotrophic lateral sclerosis. Exp Neurol 174:169–180.

Gurney ME, Pu H, Chiu AY, Dal Canto MC, Polchow CY, Alexander DD, Caliendo J, Hentati A, Kwon YW, Deng HX, Chen W, Zhai F, Sufit RL, Siddique T. 1994. Motor neuron degeneration in mice that express a human Cu,Zn superoxide dismutase mutation. Science 264:1772–1775.

Hand CK, Rouleau GA. 2002. Familial amyotrophic lateral sclerosis. Muscle Nerve 25:135–159.

Howland DS, Liu J, She Y, Goad B, Maragakis NJ, Kim B, Erickson J, Kulik J, DeVito L, Psaltis G, DeGennaro LJ, Cleveland DW, Rothstein JD. 2002. Focal loss of the glutamate transporter EAAT2 in a transgenic rat model of SOD1 mutant-mediated amyotrophic lateral sclerosis (ALS). Proc Natl Acad Sci USA 99:1604–1609.

Inoue H, Tsukita K, Iwasato T, Suzuki Y, Tomioka M, Tateno M, Nagao M, Kawata A, Saido TC, Miura M, Misawa H, Itohara S, Takahashi R. 2003. The crucial role of caspase-9 in the disease progression of a transgenic ALS mouse model. EMBO J 22:6665–6674.

Kaspar BK, Llado J, Sherkat N, Rothstein JD, Gage FH. 2003. Retrograde viral delivery of IGF-1 prolongs survival in a mouse ALS model. Science 301:839–842.

Kato M, Aoki M, Ohta M, Nagai M, Ishizaki F, Nakamura S, Itoyama Y. 2001. Marked reduction of the Cu/Zn superoxide dismutase polypeptide in a case of familial amyotrophic lateral sclerosis with the homozygous mutation. Neurosci Lett 312:165–168.

Keller JN, Huang FF, Zhu H, Yu J, Ho YS, Kindy TS. 2000. Oxidative stress-associated impairment of proteasome activity during ischemia-reperfusion injury. J Cereb Blood Flow Metab 20:1467–1473.

Landis JR, Koch GG. 1977. The measurement of observer agreement for categorical data. Biometrics 33:159–174.

Mikami Y, Toda M, Watanabe M, Nakamura M, Toyama Y, Kawakami Y. 2002. A simple and reliable behavioral analysis of locomotor function after spinal cord injury in mice. Technical note. J Neurosurg Spine 97:142–147.

Mulder DW, Kurland LT, Offord KP, Beard CM. 1986. Familial adult motor neuron disease: amyotrophic lateral sclerosis. Neurology 36:511–517.

Nagai M, Aoki M, Miyoshi I, Kato M, Pasinelli P, Kasai N, Brown RH, Jr., Itoyama Y. 2001. Rats expressing human cytosolic copper-zinc superoxide dismutase transgenes with amyotrophic lateral sclerosis: associated mutations develop motor neuron disease. J Neurosci 21:9246–9254.

Ohki-Hamazaki H, Sakai Y, Kamata K, Ogura H, Okuyama S, Watase K, Yamada K, Wada K. 1999. Functional properties of two bombesin-like peptide receptors revealed by the analysis of mice lacking neuromedin B receptor. J Neurosci 19:948–954.

Okada Y, Shimazaki T, Sobue G, Okano H. 2004. Retinoic-acid-concentration-dependent acquisition of neural cell identity during in vitro differentiation of mouse embryonic stem cells. Dev Biol 275:124–142.

Okado-Matsumoto A, Fridovich I. 2002. Amyotrophic lateral sclerosis: a proposed mechanism. Proc Natl Acad Sci USA 99:9010–9014.

Ouary S, Bizat N, Altairac S, Menetrat H, Mittoux V, Conde F, Hantraye P, Brouillet E. 2000. Major strain differences in response to chronic systemic administration of the mitochondrial toxin 3-nitropropionic acid in rats: implications for neuroprotection studies. Neuroscience 97:521–530.

Rivlin AS, Tator CH. 1977. Objective clinical assessment of motor function after experimental spinal cord injury in the rat. J Neurosurg 47: 577–581.

Rosen DR, Siddique T, Patterson D, Figlewicz DA, Sapp P, Hentati A, Donaldson D, Goto J, O'Regan JP, Deng HX, Rahmani Z, Krizus A, McKenna-Yasek D, Cayabyab A, Gasten SM, Berger R, Tanzi RE, Halperin JJ, Herzfeldt B, van den Bergh R, Hung WY, Bird T, Deng G, Mulder DW, Smyth C, Laing NG, Soriano E, Pericak-Vance MA, Haines J, Reuleau GA, Gusella JS, Horvitz HR, Brown RH Jr. 1993. Mutations in Cu/Zn superoxide dismutase gene are associated with familial amyotrophic lateral sclerosis. Nature 362:59–62.

Shipp EL, Cantini F, Bertini I, Valentine JS, Banci L. 2003. Dynamic properties of the G93A mutant of copper-zinc superoxide dismutase as detected by NMR spectroscopy: implications for the pathology of familial amyotrophic lateral sclerosis. Biochemistry 42:1890–1899.

Storkebaum E, Lambrechts D, Dewerchin M, Moreno-Murciano MP, Appelmans S, Oh H, Van Damme P, Rutten B, Man WY, De Mol M, Wyns S, Manka D, Vermeulen K, Van Den Bosch L, Mertens N, Schmitz C, Robberecht W, Conway EM, Collen D, Moons L, Carmeliet P. 2005. Treatment of motoneuron degeneration by intracerebroventricular delivery of VEGF in a rat model of ALS. Nat Neurosci 8:85–92.

Sun W, Funakoshi H, Nakamura T. 2002. Overexpression of HGF retards disease progression and prolongs life span in a transgenic mouse model of ALS. J Neurosci 22:6537–6548.

Urushitani M, Kurisu J, Tsukita K, Takahashi R. 2002. Proteasomal inhibition by misfolded mutant superoxide dismutase 1 induces selective motor neuron death in familial amyotrophic lateral sclerosis. J Neurochem 83:1030–1042.

Wang LJ, Lu YY, Muramatsu S, Ikeguchi K, Fujimoto K, Okada T, Mizukami H, Matsushita T, Hanazono Y, Kume A, Nagatsu T, Ozawa K, Nakano I. 2002. Neuroprotective effects of glial cell line-derived neurotrophic factor mediated by an adeno-associated virus vector in a transgenic animal model of amyotrophic lateral sclerosis. J Neurosci 22: 6920–6928.

Watanabe M, Aoki M, Abe K, Shoji M, Iizuka T, Ikeda Y, Hirai S, Kurokawa K, Kato T, Sasaki H, Itoyama Y. 1997. A novel missense point mutation (S134N) of the Cu/Zn superoxide dismutase gene in a patient with familial motor neuron disease. Hum Mutat 9:69–71.

Weydt P, Hong SY, Kliot M, Moller T. 2003. Assessing disease onset and progression in the SOD1 mouse model of ALS. Neuroreport 14: 1051–1054.

Williamson TL, Cleveland DW. 1999. Slowing of axonal transport is a very early event in the toxicity of ALS-linked SOD1 mutants to motor neurons. Nat Neurosci 2:50–56.

Human Molecular Genetics, 2006, Vol. 15, No. 2 **233–250**
doi:10.1093/hmg/ddi440
Advance Access published on December 1, 2005

Mice deficient in the Rab5 guanine nucleotide exchange factor ALS2/alsin exhibit age-dependent neurological deficits and altered endosome trafficking

Shinji Hadano[1,2,3,†], Susanna C. Benn[4,†], Shigeru Kakuta[5], Asako Otomo[1], Katsuko Sudo[5,‡], Ryota Kunita[1,3], Kyoko Suzuki-Utsunomiya[1], Hikaru Mizumura[3], Jeremy M. Shefner[6], Gregory A. Cox[7], Yoichiro Iwakura[5], Robert H. Brown Jr[4] and Joh-E Ikeda[1,2,3,8,*]

[1]Department of Molecular Neuroscience, The Institute of Medical Sciences and [2]Department of Molecular Life Sciences, Tokai University School of Medicine, Isehara, Kanagawa 259-1193, Japan, [3]Solution Oriented Research for Science and Technology, Japan Science and Technology Agency, Kawaguchi, Saitama 332-0012, Japan, [4]Day Neuromuscular Research Laboratory, Department of Neurology, Massachusetts General Hospital, Harvard Medical School, Charlestown, MA 02129, USA, [5]Center for Experimental Medicine, Institute of Medical Science, University of Tokyo, Tokyo 108-8639, Japan, [6]Department of Neurology, SUNY Upstate Medical University, Syracuse, NY 13104, USA, [7]The Jackson Laboratory, Bar Harbor, ME 04609, USA and [8]Department of Paediatrics, Faculty of Medicine, University of Ottawa, Ontario, Canada K1H 8M5

Received September 27, 2005; Revised and Accepted November 25, 2005

ALS2/alsin is a member of guanine nucleotide exchange factors for the small GTPase Rab5 (Rab5GEFs), which act as modulators in endocytic pathway. Loss-of-function mutations in human *ALS2* account for a number of juvenile recessive motor neuron diseases (MNDs). However, the normal physiological role of ALS2 *in vivo* and the molecular mechanisms underlying motor dysfunction are still unknown. To address these issues, we have generated mice homozygous for disruption of the *Als2* gene. The *Als2*-null mice observed through 21 months of age demonstrated no obvious developmental, reproductive or motor abnormalities. However, immunohistochemical and electrophysiological analyses identified an age-dependent, slowly progressive loss of cerebellar Purkinje cells and disturbance of spinal motor neurons associated with astrocytosis and microglial cell activation, indicating a subclinical dysfunction of motor system in *Als2*-null mice. Further, quantitative epidermal growth factor (EGF)-uptake analysis identified significantly smaller-sized EGF-positive endosomes in *Als2*-null fibroblasts, suggesting an alteration of endosome/vesicle trafficking in the cells. Collectively, while loss of ALS2 does not produce a severe disease phenotype in mice, these *Als2*-null animals should provide a useful model with which to understand the interplay between endosomal dynamics and the long-term viability of large neurons such as Purkinje cells and spinal motor neurons.

INTRODUCTION

ALS2 was initially identified as a causative gene for a juvenile recessive form of amyotrophic lateral sclerosis (ALS), termed ALS2 (OMIM 205100), in a Tunisian kindred, and a rare juvenile recessive form of primary lateral sclerosis (PLS) (PLSJ; OMIM 606353) in both Kuwaiti and Saudi Arabian consanguineous families (1,2). ALS2 is described as a spastic pseudobulbar syndrome with spastic paraplegia involving a loss of upper motor neurons (UMNs) and occasionally

*To whom correspondence should be addressed. Tel: +81 463915095; Fax: +81 463914993; Email: joh-e@nga.med.u-tokai.ac.jp
†The authors wish it to be known that, in their opinion, the first two authors should be regarded as joint First Authors.
‡Present address: Animal Research Center, Tokyo Medical University, Tokyo 160-8402, Japan.

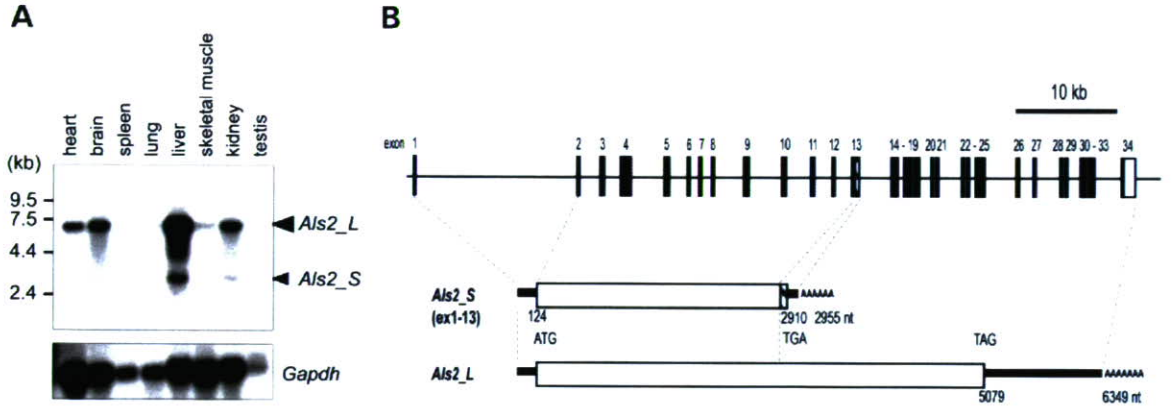

Figure 1. Expression and structure of the mouse *Als2* gene. **(A)** Northern blot analysis of the *Als2* mRNA. MTN blot (BD Biosciences) was hybridized with the *Als2* cDNA clone. Arrowheads on the right indicate the positions of major (long; *Als2_L*) and minor (short; *Als2_S*) transcripts. The lower panel represents the same blot hybridized with mouse *Gapdh* cDNA to confirm RNA quality and relative loading. Positions of size-markers are shown on the left. **(B)** Schematic representations of the genomic organization for mouse *Als2* and its transcripts. *Als2* spans ~75 kb of the genomic region and comprises 34 exons. Black and open boxes represent coding and non-coding region of the exons, respectively. A striped box represents the unique 3′-untranslated region of the *Als2_S* transcript that is produced by alternative splicing at the 5′ donor site after exon 13. Positions of translation initiation (ATG) and termination (TGA or TAG) codons are shown.

associated with several signs of lower motor neuron (LMN) defects (3), whereas PLSJ shows only UMN symptoms with no evidence of denervation (4). Recently, several independent homozygous *ALS2* mutations have also been found in families segregating an infantile-onset ascending hereditary spastic paralysis (IAHSP) (5–7), a single family of a recessive complicated hereditary spastic paraplegia (HSP) (8) and a single family of ALS2 (9). Because ALS2, PLSJ and IAHSP/HSP are group of closely related MNDs (10–13), and loss-of-function *ALS2* mutations account for a number of recessive MNDs, it is likely that the *ALS2* gene product might play an important role in motor neurons.

ALS2 encodes a novel 184 kDa protein, termed ALS2 or alsin, comprising three predicted guanine nucleotide exchange factor (GEF) domains (1,2); that is, RCC1-like domain (RLD) (14), the Dbl homology and pleckstrin homology (DH/PH) domains (15) and a vacuolar protein sorting 9 (VPS9) domain (16–21). In addition, eight consecutive membrane occupation and recognition nexus (MORN) motifs are noted in the region between DH/PH and VPS9 domains (22,23). It has previously been demonstrated that ALS2 mediates the activation of Rab5 small GTPase via its Rab5-specific GEF activity that is associated with its C-terminal MORN/VPS9 domain (22,23) and that ALS2 modulates endosome/membrane trafficking in the cells (22–26). It has also been shown that ALS2 can stimulate Rac1 (25,27,28) and promote neurite growth in neuronal cultures (28). Moreover, overexpression of ALS2 protects cultured motor neuronal cells from toxicity induced by mutant Cu/Zn-superoxide dismutase 1 (SOD1) (27,29), suggesting a possible neuroprotective role for ALS2. However, the molecular mechanisms underlying motor neuron dysfunction and degeneration in ALS2-linked MNDs are still poorly understood. Common to 10 reported *ALS2* mutations is the loss of the VPS9 domain either due to deletion (1,2,5,6,8,9) or nonsense (7) mutations in the coding exons or splicing site mutation (5,6). It is hypothesized that a perturbation of endosome and/or vesicle trafficking mediated by the ALS2-associated Rab5GEF activity underlies neuronal dysfunction and degeneration in the ALS2-linked MNDs (22,25).

To delineate the normal physiological role of ALS2 and the impact of the loss of its function *in vivo*, we have generated mice homozygous for disruption of exon 3 of the mouse *Als2* gene, and extensively characterized the resulting *Als2*-null mice. Observed through 21 months of age, these *Als2*-null mice reveal no obvious developmental or reproductive abnormalities. They also display no defects in motor performance. However, histological studies demonstrate that the *Als2*-null mice develop an age-dependent, slow loss of cerebellar Purkinje cells and evidence of subclinical dysfunction of spinal motor neurons. In addition, there is moderate astrocytosis and microglial cell activation. Cell cultural studies reveal no major abnormalities in dendrites and axons in the *Als2*-null neurons. However, there is a decrease in the size of epidermal growth factor (EGF)-positive endosomes/vesicles in the *Als2*-null fibroblasts. Taken together, our findings suggest that ALS2 is important in membrane trafficking, particularly in motor neurons and Purkinje cells, although loss of this protein does not result in a severe disease phenotype in mice. Thus, these *Als2*-null mice should provide insight into the interplay between membrane trafficking, endosomal dynamics and the long-term viability of large neurons such as Purkinje cells and spinal motor neurons.

RESULTS

Splicing and expression patterns for the mouse *Als2* transcripts are different from those for human *ALS2*

In human, the short variant of the *ALS2* transcript of ~2.6 kb, resulting from an alternative splicing at the 5′ donor site after exon 4, is rather ubiquitously expressed in various adult tissues including brain (1). Further, its expression is believed to play a role in the phenotypic variations, including ages at onset and the LMN involvement, as observed in the ALS2-linked MNDs, (1,30,31). In this study, northern blot analysis revealed that, in addition to the full-length transcript (*Als2_L*), the short variant of the mouse *Als2* transcript of an ~2.9 kb (*Als2_S*) was expressed both in liver and kidney, but was undetectable in other tissues examined including brain (Fig. 1A). BLAST searches of the GenBank/DDBJ/EMBL database and DNA sequence assembling in conjunction

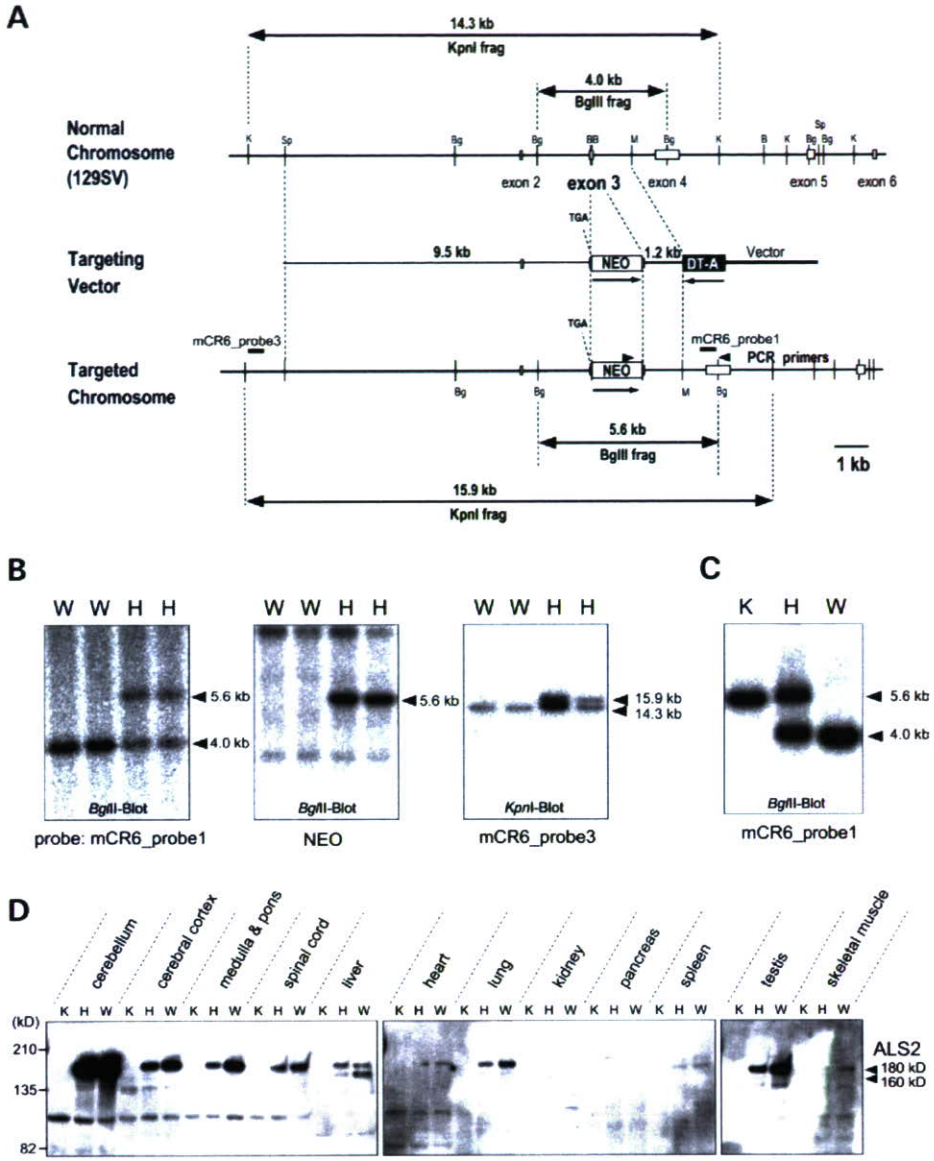

Figure 2. Targeted disruption of the mouse *Als2* gene. (**A**) Schematic representations of the targeting strategy for *Als2*. A 39 bp region flanked by two *Bam*HI sites within exon 3 of *Als2* was deleted and replaced with the neomycin gene cassette (*NEO*). The *DT-A* gene was used as a negative selection marker. Positions of two DNA probes for Southern blot analysis (mCR6_probe1 and mCR6_probe3) and PCR primers (arrowheads) both used for screening the homologous recombination are indicated. B, *Bam*HI; Bg, *Bgl*II; K, *Kpn*I; M, *Mlu*I; Sp, *Spe*I. (B and C) Southern blot analysis of genomic DNA isolated from mouse tail tissue. Genomic DNA obtained from F1 (**B**) or F2 (**C**) mice was digested with either *Bgl*II or *Kpn*I and probed with mCR6_probe1 (*Bgl*II blot), NEO (*Bgl*II blot) or mCR6_probe3 (*Kpn*I blot). The restriction fragments of 5.6 kb and 4.0 kb in *Bgl*II blot represent the targeted and wild-type alleles, respectively. The restriction fragments of 15.9 and 14.3 kb in *Kpn*I blot represent the targeted and wild-type alleles, respectively. K, homozygous mutant ($Als2^{-/-}$); H, heterozygous mutant ($Als2^{+/-}$); W, wild-type ($Als2^{+/+}$). (**D**) Western blot analysis of ALS2 expression in various tissues from $Als2^{-/-}$ (K), $Als2^{+/-}$ (H) and $Als2^{+/+}$ (W) mice. Equal amount of protein (30 μg) was loaded in each lane, and the anti-ALS2 polyclonal antibody (HPF1-680) was used to probe ALS2 (180 kDa), a product of the major *Als2_L* transcript, indicated on the right. The positions of size-markers are shown on the left.

with an extensive reverse transcriptase (RT)–Polymerase chain reaction (PCR)-based cloning identified the *Als2* short variant of 2955 nt with a single 2787 nt ORF encoding 928 amino acids (~100 kDa) (GenBank accession no. BC031479) (32) and revealed that *Als2_S* was produced by alternative splicing at the 5′ donor site after exon 13, resulting in a premature stop codon after 74 amino acid residues in intron 13 (Fig. 1B). Thus, the structure and expression pattern for the mouse *Als2* short transcript are different from that for the human variant.

Als2 mutant mice are viable and appear to develop normally

To generate *Als2*-null mice, we constructed a targeting vector in which exon 3 of the *Als2* gene was disrupted by inserting a stop codon, followed by the neomycin resistance gene transcribed under the control of the *Pkg1* promoter (Fig. 2A), which allowed to disturb the normal expression of both *Als2_L* and *Als2_S* transcripts. Although the *Als2* gene in a targeted allele can be transcribed by its own promoter,

the protein translation is terminated after the first 14 amino acids; as a result, the peptide lacks all the functional domains for ALS2. Six of 14 homologous recombinant ES clones exhibiting the desired targeting event were selected and subjected to the generation of chimera mice. Two germline chimeras (clones 17C6 and 21B5) were identified by analyzing the F1 animals, which were produced by crossing each male chimera with female C57BL/6J mouse, using PCR (data not shown) and Southern blotting (Fig. 2B). F1 mice heterozygous for the *Als2* mutation ($Als2^{+/-}$) derived from clone 17C6 were interbred, generating F2 ($n = 237$) and F3 ($n = 42$) mice for the analysis. The homologous recombination event in F2/F3 animals was also confirmed by Southern blot analysis (Fig. 2C). Further, western blot analysis of various tissues using two independent anti-ALS2 antibodies, HPF1-680 and MPF1012-1651, demonstrated that the expression of ALS2, a product of *Als2_L*, was eliminated in the *Als2* homozygous mutant mice, and also reduced by approximately half in the heterozygous mutant mice (HPF1-680, Fig. 2D; MPF1012-1651, Supplementary Material, Fig. S1). However, no band corresponding to the predicted mouse short ALS2 variant (~100 kDa) was observed using our anti-ALS2_RLD antibody (HPF1-680) (Fig. 2D). Collectively, the homozygous *Als2* mutant animals created in this study can be considered to recapitulate the status of null-expression of ALS2 in ALS2-linked MND patients.

The *Als2*-null mice were viable and fertile with no evidences for motor abnormality as observed for at least 21 months of age. The mutant allele was transmitted in the expected Mendelian ratio of an autosomal gene [$Als2^{-/-}$ (homozygote), $n = 72$ (25.8%), male (m)/female (f) = 30/42; $Als2^{+/-}$ (heterozygote), $n = 128$ (45.9%), m/f = 71/57; $Als2^{+/+}$ (wild-type), $n = 79$ (28.3%), m/f = 42/37]. Further, growth of both homozygous and heterozygous mice assessed by the changes in their body weight was not statistically different from that of their wild-type littermates, despite that a number of *Als2*-null female mice exhibited an excessive body weight (Fig. 3A). Survival data at the age of 92 weeks also revealed no statistical differences between the genotype groups, although a slightly lower rate of survival in homozygous mutants were observed (Fig. 3B).

Als2 mutant mice display no profound defects in motor performance

Repeated examination of the selected F2 mice ($n = 9$ for each genotype group) on the accelerating rotarod test over a period of 81 weeks with a weekly testing frequency revealed that the rotarod performance among animals varied irrespective of their genotypes. Although the wild-type and *Als2* heterozygous mice showed a tendency toward improved performance when compared with the *Als2* homozygotes, this was not statistically significant (Fig. 3C). Further, preliminary analysis of the cage activities in these mice, measured by a SUPERMEX system with an infrared ray sensor monitor (Muromachi Kikai), also showed no statistically significant differences in the spontaneous motor activities between groups (data not shown).

Lack of ALS2 does not affect expression levels of proteins related to the cytoskeleton and membrane trafficking

To test whether lack of ALS2 expression affect a series of 33 cytoskeletal or membrane/vesicle associated proteins, including Rab5 and Rac1, both of which were known to bind to ALS2 (22,23,25,27), and ALS2CL, a novel ALS2 homologous protein (33), we conducted western blot analysis of extracts obtained from brain (cerebral cortex, cerebellum, medulla/pons and spinal cord), liver and kidney (8 and 24 weeks of age, Supplementary Material, Fig. S2; 72 weeks of age, Supplementary Material, Fig. S3). Among the proteins tested, the levels of early endosome antigen 1 (EEA1), a Rab5-effector downstream of ALS2 (22,34), of the 8- and 24-week-old homozygous and heterozygous mutant mice were slightly decreased in cerebral cortex, but not in cerebellum. Furthermore, the levels of neurofilament heavy chain were slightly increased in spinal cord of the 72-week-old homozygous and heterozygous mutant mice. However, none of other proteins, including Rab5, Rabaptin-5, Rab4, α-tubulin, β-tubulin, MAP2, α-adaptin, amphiphysin, AP180, clathrin HC, Rac1, Rab3, Rab8, Rab11, β-catenin, EGF, complexin II, Mint2, Munc-18, rabaphilin 3A, rSec8, SNAP25, synapsin I, synapsin IIa, synaprogyrin, synaptophysin, synaptotagmin, syntaxin 6, GRP78 and ALS2CL showed altered levels of expression.

Brain and spinal cord of the *Als2* mutant mice are histologically normal

ALS2 immunostaining was observed in the cerebellum, brainstem and spinal motor neurons of wild-type but not *Als2*-null mice (Fig. 4A–I). ALS2 is highly expressed in the granular and Purkinje layers of wild-type mice (Fig. 4C and F) and colocalizes with some, but not all calbindin immunopositive Purkinje cells (Fig. 4J). High magnification of Purkinje and spinal cord demonstrate cytoplasmic ALS2 immunostaining (Fig. 4F′ and H′), with a dense localization to perinuclear membranous compartments in spinal motor neurons (Fig. 4H′). Low level ALS2 expression was also detected in CA2 of the hippocampus and motor cortex (data not shown). A comparable pattern of immunostaining was obtained on brain sections from wild-type mice using an independent anti-ALS2 antibody (HPP1024) (22) (Supplementary Material, Figs S4–S6). Double immunostaining with anti-ALS2 and anti-calbindin confirmed that ALS2 is expressed in subpopulations of Purkinje and surrounding cells in wild-type animals (Fig. 4J and J′; Supplementary Material, Figs 5 and 6). Hematoxylin and eosin (H&E) morphological staining for mid-brain (Fig. 4M and O), cerebellum (Fig. 4N and P) and spinal cord (Fig. 4S–V) demonstrated no gross abnormality and neuronal lesion phenotype in *Als2*-null mice at 7 months of age.

Cerebellar Purkinje cells are significantly decreased in the aged *Als2*-null mice

Immunohistochemial analysis revealed that the density of calbindin positive Purkinje cells in cerebellum of aged *Als2*-null mice (18 months of age) was significantly decreased (Fig. 4L). A higher-magnification analysis of the Purkinje cell layers

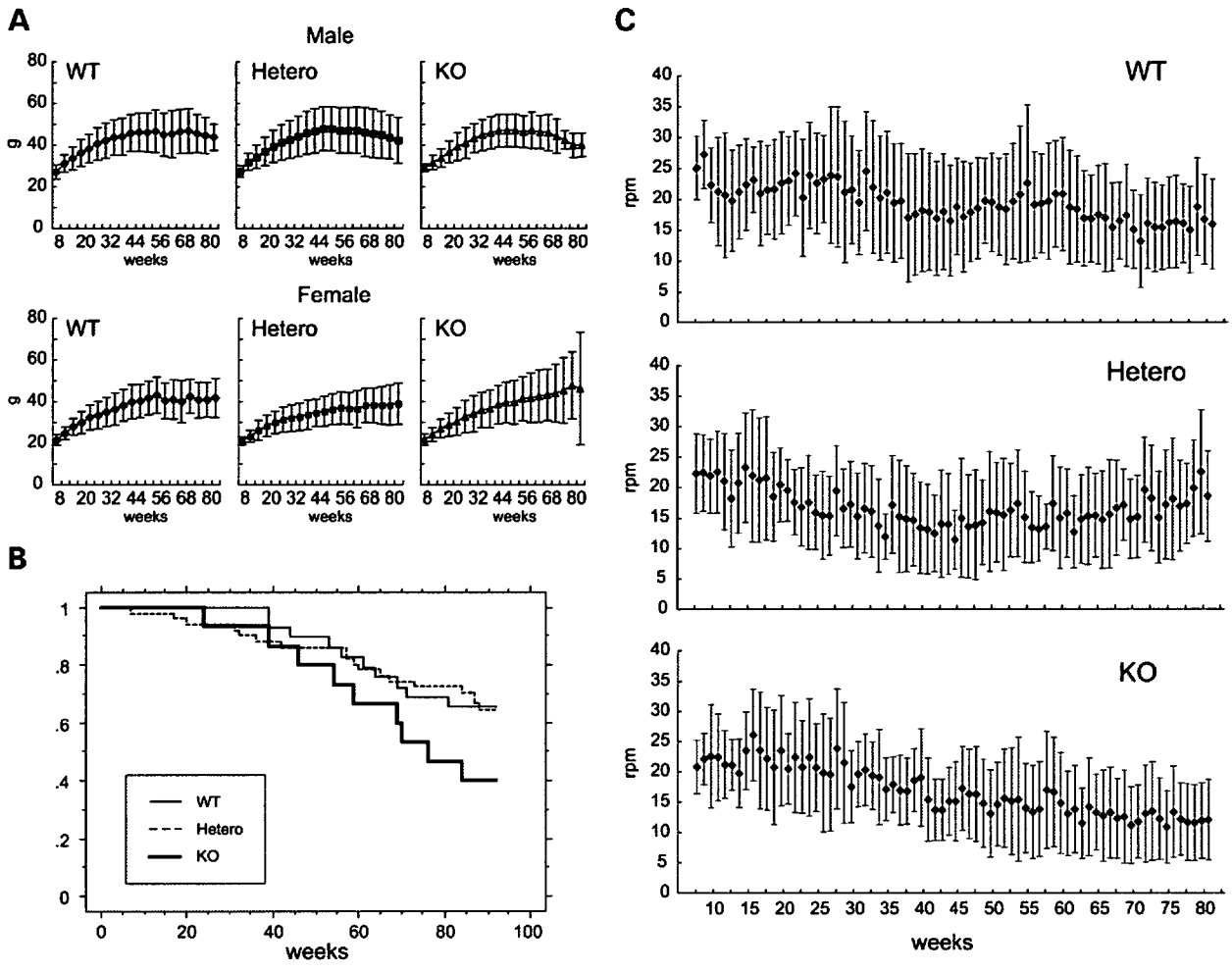

Figure 3. Gross phenotypes of the *Als2* mutant mice. (**A**) Growth curves for homozygous mutant ($Als2^{-/-}$; KO), heterozygous mutant ($Als2^{+/-}$; Hetero) and wild-type ($Als2^{+/+}$; WT) mice. The number of animals at each time point range as follows: male: WT ($n = 10$–35), Hetero ($n = 21$–51), KO ($n = 3$–22); female: WT ($n = 9$–29), Hetero ($n = 16$–46), KO ($n = 4$–32). Data are presented as means ± SD. No significant differences between genotype groups were observed (ANOVA). (**B**) Survival curves for homozygous mutant ($Als2^{-/-}$; KO, $n = 15$), heterozygous mutant ($Als2^{+/-}$; Hetero, $n = 51$) and wild-type ($Als2^{+/+}$; WT, $n = 29$) mice at the age of 92 weeks. Kaplan–Meier analysis identified no significant differences between groups ($P = 0.1832$ by log-rank test), despite a trend toward slightly reduced viability of the *Als2*-null mice was observed. (**C**) Motor performance of homozygous mutant ($Als2^{-/-}$; KO, $n = 9$), heterozygous mutant ($Als2^{+/-}$; Hetero, $n = 9$) and wild-type ($Als2^{+/+}$; WT, $n = 9$) mice on an accelerating rotarod apparatus. Data are presented as means ± SD. Repeated-measures ANOVA confirmed no significant genotype effect at each time point analyzed.

confirmed this finding (Fig. 4Q and R). To determine whether loss of ALS2 expression grossly affects viability and the spatial pattern of Purkinje cells, an estimation of Purkinje cell number was conducted by counting calbindin immunopositve Purkinje cells in the cerebellum of *Als2*-null and wild-type mice using the BIOQUANT system (Fig. 5). The results showed that, at 7 months of age, there was no significant difference either of number or of area of Purkinje cells between wild-type and *Als2*-null mice (Fig. 5A and B). However, consistent with the results of immunohistochemistry, a 22.9% decrease in the number of Purkinje cells was observed in *Als2*-null mice ($n = 3$) at 18 months of age. Thus, there were 25.74 ± 1.56 SE Purkinje cells per 1 mm length of Purkinje layer in *Als2*-null mice compared to 33.36 ± 1.34 SE cells in age-matched wild-type mice ($n = 3$, Fig. 5A) ($P = 0.023$, ANOVA). In addition, there was a 30.5% reduction in cell soma size of Purkinje cells in *Als2*-null mice ($n = 3$), with a mean soma area of 135.3 ± 5.1 SE μm^2 compared with 194.6 ± 13.1 SE μm^2 soma size in wild-type mice ($n = 3$, Fig. 5B) ($P = 0.013$, ANOVA). Representative images of the calbindin immunostaining for the cerebellum of wild-type (Fig. 5C and C′) and *Als2*-null (Fig. 5D and D′) mice at 18 months of age were shown. Together, the results are indicative of a slow progressive loss of cerebellar Purkinje cells in *Als2*-null mice.

Astrocytosis and microglial activation are progressively enhanced in the *Als2* mutant mice brain and spinal cord

In comparison with wild-type, age-matched control mice, brain and spinal cord of *Als2*-null mice at 7 and 18 months of age revealed significant progressive increases in the intensities of immunostaining for GFAP, CD68 and CD11b, markers for astrocytes, activated microglia and macrophages,

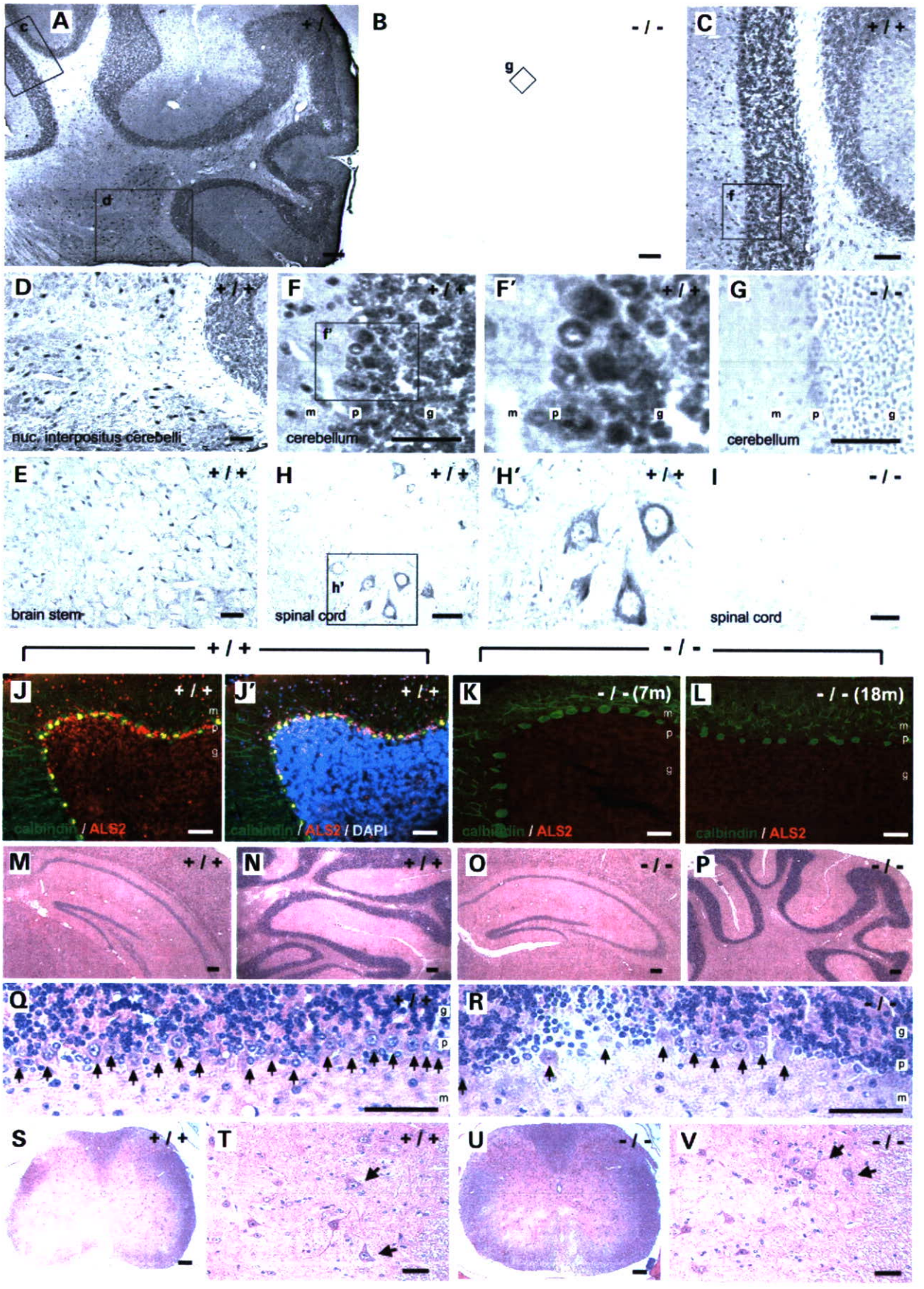
A
+/+
B
-/-
C
+/+
c
d
g
f
D
+/+
nuc. interpositus cerebelli
F
+/+
f'
m
p
g
cerebellum
F'
+/+
G
-/-
cerebellum
E
+/+
brain stem
H
+/+
h'
spinal cord
H'
+/+
I
-/-
spinal cord
+/+
-/-
J
+/+
calbindin / ALS2
J'
+/+
calbindin / ALS2 / DAPI
K
-/- (7m)
calbindin / ALS2
L
-/- (18m)
calbindin / ALS2
M
+/+
N
+/+
O
-/-
P
-/-
Q
+/+
R
-/-
S
+/+
T
+/+
U
-/-
V
-/-

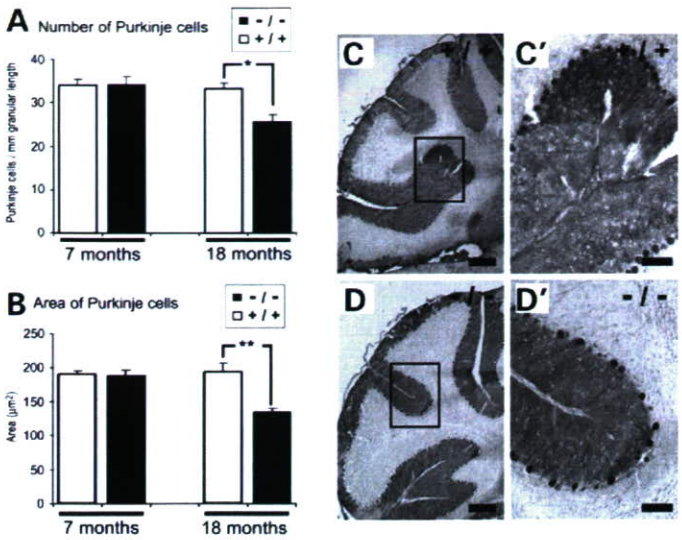

Figure 5. The number of Purkinje cells in the cerebellum of *Als2*-null mice is decreased. (**A** and **B**) Mean estimates of Purkinje cell number (A) and soma size (B) in wild-type (+/+) and *Als2*-null (−/−) mice ($n = 3$ per group) at 7 and 18 months of age, represented as the mean density of Purkinje cells per 1 mm length of Purkinje cell layer (A) and mean soma area (B). Data are presented as means ± SE. $^{*}P = 0.023$, $^{**}P = 0.013$ (ANOVA) of *Als2*-null versus wild-type control. (**C** and **D**) Anti-calbindin immunostaining of sagittal cerebellum sections of wild-type (C) (higher magnification C′) and *Als2*-null mice (D) (higher magnification D′) at 18 months of age. [Scale bars = 200 μm (C and D); 50 μm (C′ and D′).]

respectively (Fig. 6). This strongly suggests that there is an increase in astrogliosis and activation of inflammatory responses in *Als2*-null mice. Immunostaining for the neuronal markers SMI32 was normal in *Als2*-null mutants both at 7 and 18 months of age (Fig. 6A–D).

Als2-null mice show evidences for motor unit remodeling

To determine whether there is a functional impairment in LMN of *Als2*-null mice, we have conducted motor unit number estimation (MUNE) analysis. The mean of estimated total number of viable axons (motor units) in the distal hind limb, determined by MUNE, is significantly reduced from 274.5 (±29.1) in wild-type mice ($n = 5$) to 208.5 (±50.8) in *Als2*-null mutant mice ($P = 0.022$; $n = 4$) at 12 months of age (Fig. 7A). Concurrently, the single motor unit potential (SMUP) increases from 0.156 mV (±0.032) in wild-type mice to 0.178 mV (±0.037) in *Als2*-null mutant mice (Fig. 7B), reflecting an increase in the response of a single motor unit with decreasing MUNE. A similar pattern was observed in a single *Als2*-null mutant at 20 months of age, with mean MUNE and SMUP values of 191.0 (±0.76) and 0.225 (±0.165), respectively, compared with 285.3 (±0.76) and 0.145 (±0.023) in age-matched wild-type animals ($n = 3$). This decrease in MUNE and concurrent increase in SMUP amplitude is consistent with remodeling of the architecture of the motor unit in *Als2*-null mice, with cycles of motor neuron degeneration leading to denervation followed by reinnervation. This process reduces the number of motor units (MUNE) but increases the mean size of the remaining motor units (SMUP).

Ventral motor axons are significantly decreased in *Als2*-null mice

In the *Als2*-null mice, quantitative histological analysis of the numbers of axons in the L4 ventral root failed to demonstrate any change in the numbers of the large motor neurons (>5 μm; the alpha motor neuron category) or small motor neurons (in the gamma motor neuron category with axon diameters between 1.4 and 4.5 μm) at 7 months of age ($n = 3$ per group) (Fig. 7C and D). However, analysis of *Als2*-null mutants at 18 months of age ($n = 3$) showed a significant decrease in the numbers of axons of all sizes (Fig. 7E and F) in particular small motor neurons with axon diameters between 1.5–4.5 μm. These morphometric findings suggest that there has been a progressive loss of motor axons of *Als2*-null animals.

Als2-null mice show evidence of fiber redistribution in skeletal muscle

To investigate the effect of ALS2 loss on skeletal muscle integrity, the morphology of muscle fibers and fiber types was examined in gastrocnemious and quadriceps muscles. No major difference was observed in H&E or acetylcholinesterase histochemistry stain of transverse gastrocnemius muscle of wild-type or *Als2*-null mice at 7 and 20 months of age (data not shown), although examination of thoracic muscle from *Als2* mutant mice occasionally showed some isolated, angular atrophic muscle fibers and regions of dense pyknotic nuclear clumping and central nuclei suggestive of denervation (data not shown). Interestingly, myosin-ATPase (pH 4.3) staining revealed a slight redistribution and fiber grouping of dark (Type I, slow) myofibrils in the gastrocnemius muscle from the *Als2*-null mice at 7 months, with a severely abnormal pattern of fiber distribution at 20 months of age compared with wild-type (Fig. 7G–J). Again, these histochemical data are consonant with the electrophysiological

Figure 4. Gross morphology and immunohistochemistry of ALS2 in the brain and spinal cord of wild-type and *Als2*-null mice. (**A**–**I**) Immunostaining of sagittal brain paraffin sections with anti-ALS2 antibody (HPF1-680) of wild-type cerebellum and brainstem (**A**) compared to a comparable brain region of *Als2*-null mice at 7 months of age (**B**). ALS2 immunoreactivity is observed in the cerebellum (**A**, **C** and **F**) (at high magnification shown in **F** and **F′**), nucleus interpositus cerebelli (**D**) and brainstem (**E**), as well as in motor neurons in the lumbar spinal cord (**H**) (at higher magnification **H′**) in wild-type (+/+) but not *Als2*-null (−/−) mice at 7 months of age (I). (**J**–**L**) Double immunostaining with anti-ALS2 (red) and anti-calbindin (green) of granular region of cerebellum of wild-type (**J**) and composite image with DAPI (blue) (**J′**) and *Als2*-null mice at 7 months (**K**) and 18 months of age (**L**). ALS2 expression is detected in the granular (g) and Purkinje (p) layer in the cerebellum and colocalizes with many, but not all calbindin positive Purkinje cells (white arrow). (**M**–**V**) H&E morphological stain of mid-brain (**M** and **O**), cerebellum (**N** and **P**) and spinal cord (**S**–**V**) of wild-type and *Als2*-null mice at 7 months of age. Arrows in (**Q** and **R**) show Purkinje cells and indicate the irregular distances between Purkinje cells in *Als2*-null mice at 18 months of age (R). Arrows illustrate spinal cord motor neurons (**T** and **V**). m, molecular layer; p, Purkinje layer; g, granular layer. [Scale bars = 100 μm (**A**, **B**, **M**–**P**, **S** and **U**); 50 μm (**C**–**L**, **Q**, **R**, **T** and **V**).]

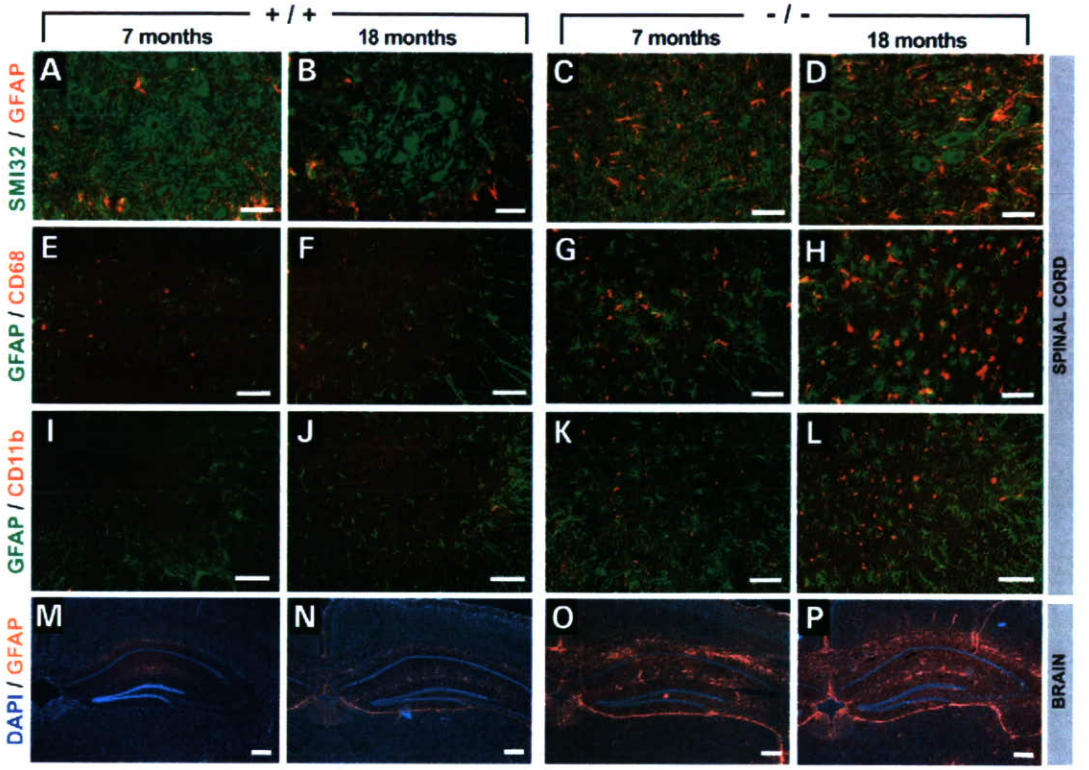

Figure 6. Astrocytosis and microglial activation are enhanced in the *Als2* mutant mice brain and spinal cord. Composite images of double immunolabelling of lumbar spinal cord (**A**–**L**) and hippocampus (**M**–**P**) from wild-type (+/+) and *Als2*-null (−/−) mice at 7 and 18 months of age. Double immunostaining for GFAP (astrocyte marker) with SMI32 (neuronal marker) (**A**–**D**), CD68 (activated microglia) (**E**–**H**), CD11b (macrophages) (**I**–**L**) of spinal cord from wild-type and *Als2*-null mice. Hippocampus brain regions immunostained for GFAP and counterstained with DAPI (**M**–**P**). [Scale bars = 50 μm (**A**–**L**); 100 μm (**M**–**P**).]

analysis, suggesting the occurrence of some denervation of scattered motor units followed by reinnervation.

Neuromuscular junctions of *Als2*-null mice are morphologically abnormal

We have also performed a qualitative analysis of the neuromuscular junctions (NMJs) by staining post-synaptic acetylcholine receptors with fluorescently labeled, α-bungarotoxin (αBTX). These studies showed that there were fewer NMJs detected by αBTX staining of gastrocnemius muscle in *Als2*-null mice at 12 (data not shown) and 20 months of age when compared with wild-type controls (Fig. 7K and L). Interestingly, in 20-month-old *Als2*-null mice, the post-synaptic folding within the NMJ appeared to be less complex, of smaller size and somewhat more globular conformation (Fig. 7N) when compared with normal endplate formation in age-matched wild-type muscle (Fig. 7M). Again, these findings are consistent with a chronic, slowly progressive impairment of function of the distal motor terminal and altered integrity of the NMJ.

Primary neuronal cells derived from *Als2*-null mutant mice grow and differentiate normally

Previous studies using primary neuronal cultures have demonstrated that ALS2 is localized within small punctate structures throughout the cells (25), suggesting that it functions in endosomes, possibly mediating vesicle trafficking in neurons (22). As the rearrangement of cytoskeletons and membrane trafficking is thought to play major roles for the neuronal differentiation/polarization (35), we have investigated the role of ALS2 in growth and maturation of neuronal cells in detail and the impacts of its functional loss in neurons. Primary hippocampal neuronal cultures from E18 *Als2*-null mice and their wild-type littermates on a mixed genetic background (F2) were prepared and maintained. The results showed that both cultured neurons were normally differentiated (stages 3–4/DIV 4.5) (Fig. 8A, upper panels) and displayed the fully elaborated MAP2-positive neurites (dendrites) at a late stage (stage 5/DIV21) (Fig. 8A, lower panels). Further, branching numbers of dendrites were also normal in *Als2*-null neurons (data not shown). The results suggest that ALS2 is dispensable for the neurite/dendrite formation in hippocampal neurons.

Next, to examine whether loss of ALS2 affects the formation of axon in neurons, quantitative analysis of the axonal sprouting was performed using primary granule neurons. Granule neuronal cultures were established from cerebellum of P6 homozygous mutant ($n = 3$), heterozygous mutant ($n = 11$) and wild-type ($n = 4$) animals, which were produced by intercrossing the fourth-backcrossed generations (N4). Representative images of the primary granule cells (4 h after plating) were shown (Fig. 8B). Approximately 40% of the granule cells showed a sprouting phenotype, but no significant differences in their frequencies were observed among the different genotype groups (Fig. 8C).

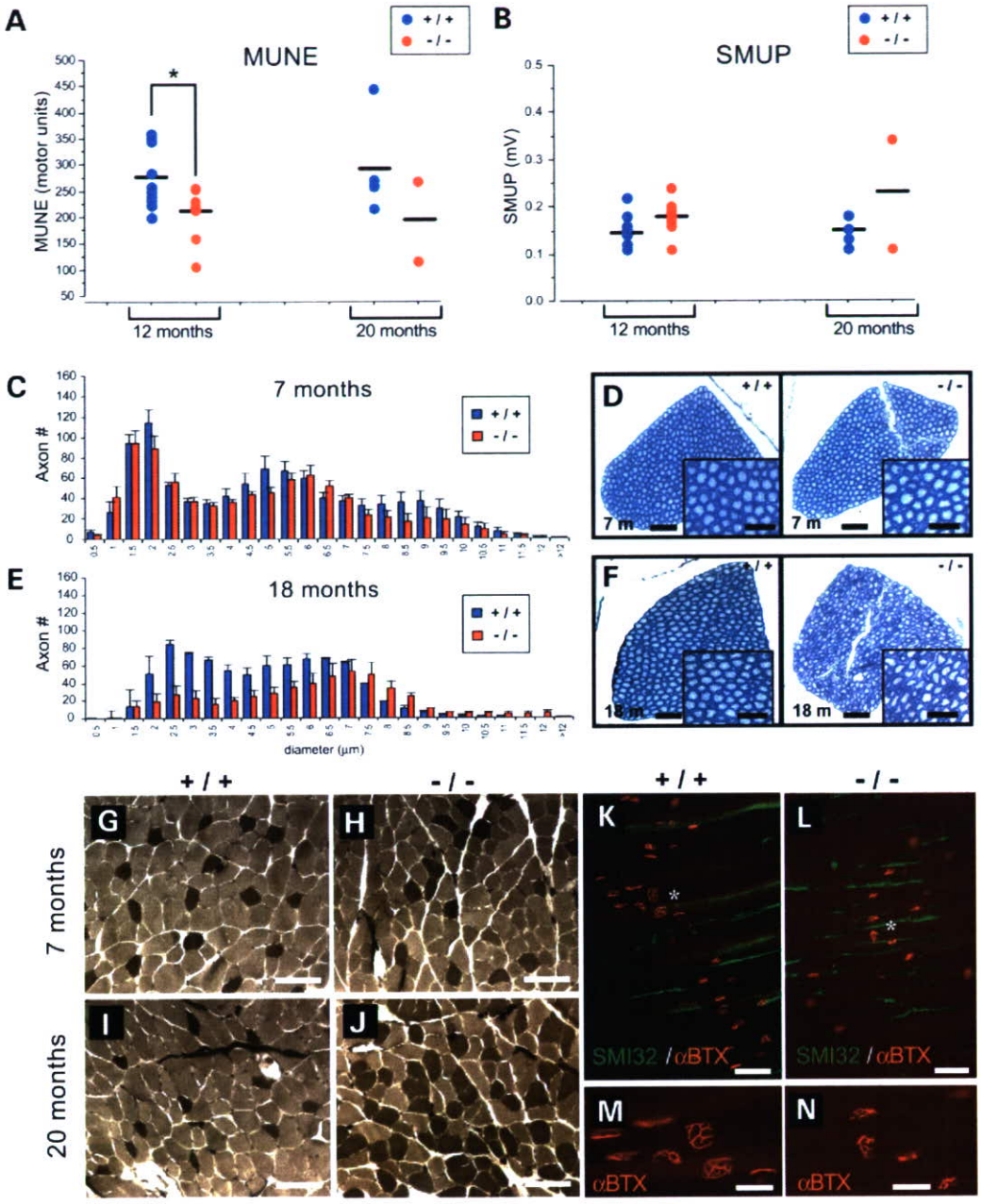

Figure 7. *Als2*-null mice exhibit late-onset partial degeneration of muscle. (**A** and **B**) MUNE (**A**) and SMUP (**B**) of wild-type (+/+, blue dots) and *Als2*-null mice (−/−, red dots) at 12 and 20 months of age ($n = 5$ and 3 for wild-type mice and $n = 4$ and 1 for *Als2*-null mice at 12 and 20 months, respectively). Black bars represent the mean MUNE or SMUP for each genotype, respectively. $^*P = 0.022$ (ANOVA) of *Als2*-null versus wild-type control. (**C**–**F**) Quantitative analysis of L4 ventral roots of wild-type (blue bars) and *Als2*-null mice (red bars) at 7 months (**C**) and 18 months (E) of age ($n = 3$ per group). Data are presented as means ± SE. Toluidine blue staining of representative L4 ventral root diameters from wild-type and *Als2*-null mice at 7 months (**D**) and 18 months (**F**), respectively, with high magnification inset. (**G**–**J**) Myosin-ATPase (pH4.3) histochemistry of transverse gastrocnemius muscle from 12- and 20-month-old wild-type (**G** and **I**) and *Als2*-null (**H** and **J**) mice. (**K**–**N**) Post-synaptic endplates at the NMJs are stained with αBTX to mark synapses (red) and SMI32 (green) to define axons in longitudinal sections from gastrocnemius muscle from wild-type (**K**) and *Als2*-null (**L**) mice at 20 months of age, with high magnification of the region marked by a white asterisk in (**M**) and (**N**), respectively. [Scale bars = 100 μm (**G**–**J**); 50 μm (**D**, **F** and **M**–**N**); 20 μm (insets in **D** and **F**).]

Endosome dynamics are slightly affected by the *Als2* mutation in fibroblasts

To further investigate the effects of ALS2 absence on cellular function, particularly receptor-mediated endocytosis in detail, we have prepared primary fibroblasts from new-born $Als2^{-/-}$ and $Als2^{+/+}$ littermates, which were produced by intercrossing the N4 backcrossed heterozygous mutant mice. Fibroblasts were exposed to Alexa Fluor-488 labeled EGF for 10 min, allowing the internalization of EGF via receptor-mediated endocytosis, and then analyzed at 10, 30 and 60 min time points. Internalized EGF forms a punctate pattern of vesicles,

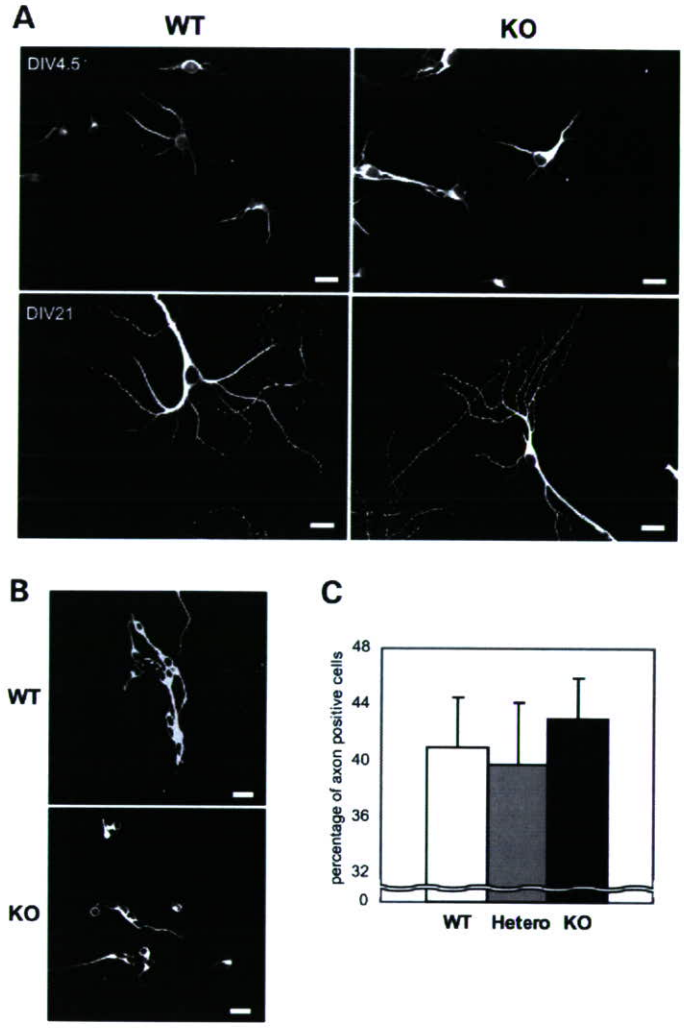

Figure 8. Primary neuronal cultures derived from *Als2*-null mutant mice are grown and differentiated. (**A**) Primary hippocampal neuronal cultures from E18 *Als2*-null mice (KO) and their wild-type littermates (WT) on a mixed genetic background (F2). Two representative stages of the cultures stained with anti-MAP2 antibody are shown (upper panels, stages 3–4/DIV 4.5; lower panels, stage 5/DIV21). (**B**) Primary cerebellar granule cell cultures from P6 *Als2*-null mice (KO) and their wild-type littermates (WT) on an N4-backcrossed background. Representative images of the primary granule cells (4 h after plating) stained with anti-βIII tubulin antibody are shown. (**C**) A quantitative analysis of the axonal sprouting in primary granule neurons. Granule neurons were established from cerebellum of P6 homozygous mutant ($n = 3$), heterozygous mutant ($n = 11$) and wild-type ($n = 4$) animals. The number of the cells with a sprouting axon was counted by observing 100 cells in every preparation. A total of 300 homozygous, 1100 heterozygous and 400 wild-type cells were analyzed. Values are expressed as means ± SE (WT, 41.0 ± 3.5%; Hetero, 39.7 ± 4.4%; KO, 43.0 ± 2.9%). Scale bars = 20 μm.

representing EGF-positive endosome compartments. No gross abnormality was observed at all time points analyzed both in *Als2*-null and wild-type cells. These results imply that endocytosis of the EGF receptor *per se* does not require ALS2 (Fig. 9A). However, a quantitative analysis of the fluorescence intensities of the EGF-labeled endosomes/vesicles revealed that frequency of the vesicles with stronger fluorescent signals, thus larger in size, was significantly lower at a 10 min point in the *Als2*-null mutants than in the wild-type cells (Fig. 9B and C, $P = 0.045$ by *t*-test). Notably, signal intensities in the wild-type cells were gradually decreased thereafter, whereas those in *Als2*-null mutants rather increased with highest at a 30 min point (Fig. 9C). The results imply that trafficking and fusion of EGF-positive endosomes/vesicles in fibroblasts were significantly delayed by the lack of ALS2. Thus, ALS2 might control efficiency of vesicles/endosomes trafficking and fusion in the cells.

DISCUSSION

Thus far, 10 independent homozygous *ALS2* mutations have been reported, which include a single-nucleotide deletion in exon 3 of the *ALS2* gene that was originally found in Tunisian ALS2 patients (1,2), and nine additional independent mutations in families segregating ALS2, PLSJ and IAHSP/HSP (1,2,5–9). Interestingly, there are recognizable phenotypic differences between ALS2 and PLSJ/IAHSP, in which ALS2 patients develop a spastic pseudobulbar syndrome with spastic paraplegia involving a loss of UMN and occasionally associated with several signs of LMN defects (3,9), whereas those with PLSJ or IAHSP/HSP shows only UMN symptoms with no evidence of denervation (4,6). Although the molecular basis underlying such phenotypic differences is still obscure, it is tempting to speculate that the expression of a short variant of the *ALS2* gene is believed to play a role in the phenotypic variations (1,30,31). We reasoned that generating mice homozygous for disruption of exon 3 of the mouse *Als2* gene resembling the Tunisian ALS2 mutation would delineate disease pathogenesis for MNDs involving loss of both UMN and LMN.

Our gene targeting strategy has been designed to disrupt the expression not only of the full-length *Als2* transcript but also a newly identified ~2.9 kb short variant of *Als2* (*Als2_S*), which is otherwise expressed predominantly in liver and kidney. Southern and Western blot analyses clearly demonstrated a complete loss of the functional full-length ALS2 protein in $Als2^{-/-}$ mice. We also identified a loss of expression of *Als2_S* in the $Als2^{-/-}$ mice (data not shown), while there is no explicit evidence for its expression at the protein level even in the wild-type animals (Fig. 3D). Taken together, our *Als2* knockout mice represent a genuine *Als2*-null lacking the expression of the functional ALS2 protein.

To our surprise, the *Als2*-null mice and the *Als2* heterozygotes have demonstrated normal growth, reproductivity, survival and motor performance. Biochemical and histological examinations also revealed no profound abnormalities in the brain and spinal cord of the *Als2*-null mice. Further, cell cultural studies showed no abnormal growth and differentiation of dendrites and axons in *Als2*-null primary neurons. Most recently, Cai *et al.* (36) reported that similar *Als2*-null mice do not demonstrate major motor deficits, but have a moderate, age-dependent impairment in motor coordination and motor learning, a higher level of anxiety response, increased body weight and increased susceptibility to oxidative stress. Although our results did not reach a statistical significance, tendencies in the decreased levels of motor coordination and increased body weight in female *Als2*-null mice are consistent with their results. At this stage, we cannot formally exclude the possibility that the phenotypic variations observed in

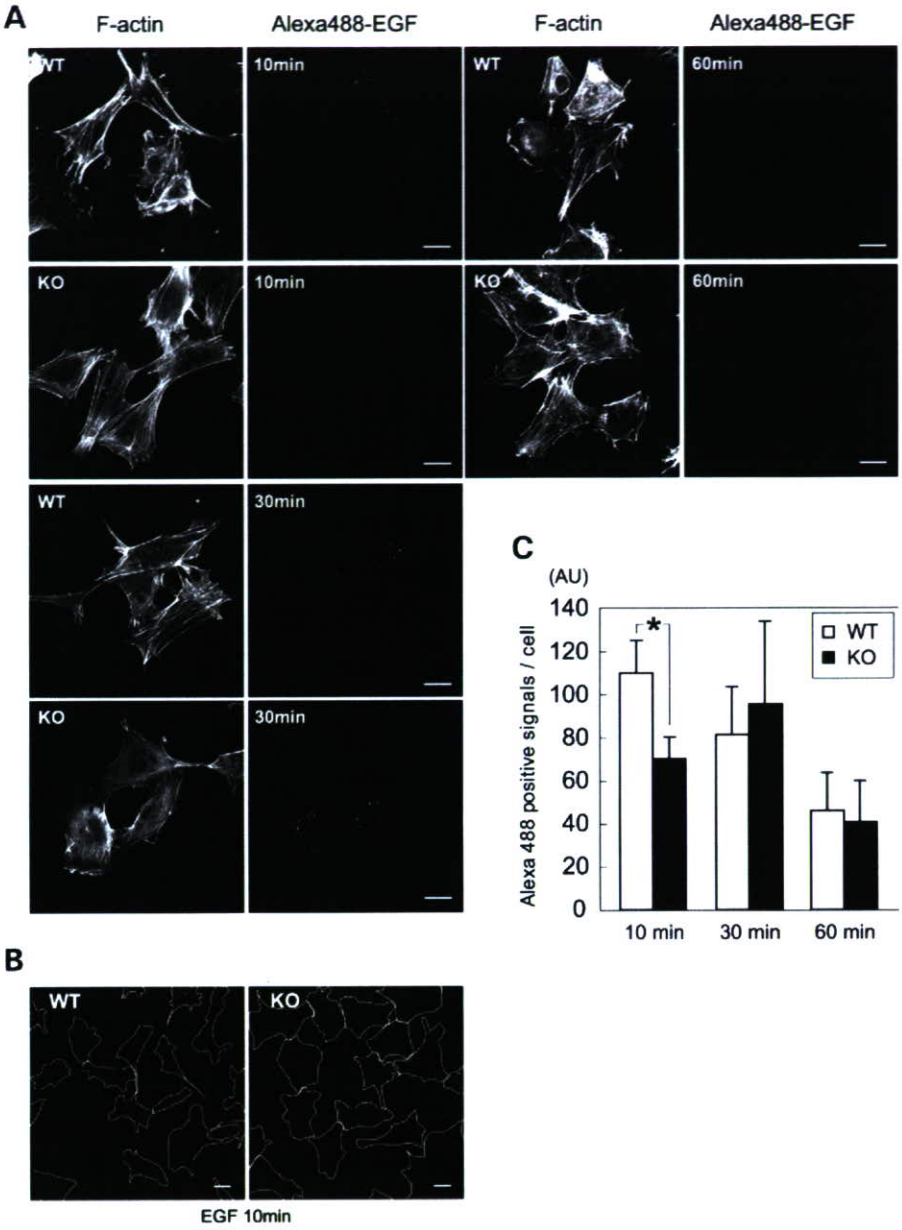

Figure 9. Endocytosis and endosome trafficking in *Als2*-null fibroblasts. (**A**) Immunofluorescence of EGF internalization in wild-type (WT) and *Als2*-null (KO) fibroblasts. Cells were starved for 2 h, exposed to Alexa Fluor-488 labeled EGF for 10 min and observed for immunofluorescence through 60 min. Cells were visualized by Alexa Fluor-594 labeled Phalloidin staining. Representative fields as shown as observed at 10, 30 and 60 min are shown. (**B**) Representative images for the digitally demarcated fibroblasts. There are no significant differences in the areas of the cells between genotype groups [WT versus KO; 28 696 $\pm$ 17 271 pixels ($n = 66$) versus 29 165 $\pm$ 10 383 pixels ($n = 60$); means $\pm$ SD]. (**C**) Quantitation of the fluorescence intensities of the EGF-labeled endosomes/vesicles in fibroblasts of wild-type (open bars) and *Als2*-null mice (filled bars) after 10, 30 and 60 min of EGF internalization. The *y*-axis represents the cumulative intensity of fluorescence (AU; arbitrary unit) in the single cell [at 10 min: WT versus KO, 110.1 $\pm$ 14.6 AU ($n = 73$) versus 70.2 $\pm$ 9.5 AU ($n = 103$); at 30 min: WT versus KO, 81.6 $\pm$ 21.5 AU ($n = 57$) versus 95.7 $\pm$ 37.4 AU ($n = 43$); at 60 min: WT versus KO, 46.0 $\pm$ 17.2 AU ($n = 32$) versus 40.7 $\pm$ 18.6 AU ($n = 26$)]. Values are expressed as means $\pm$ SE, $^*P = 0.045$ by *t*-test.

Als2-null mice are due to a strain effect, because most of the analyses were conducted using F2 mice on a mixed genetic background, in which knockout mice show a flanking gene effect with the 129/Ola genetic context than wild-type littermates (37). To address this further, we are characterizing the *Als2*-null mice generated by backcrossing $\sim$10 generations with either C57BL/6J or FVB/N mice. Nonetheless, both data suggest that the *Als2* gene *per se* is dispensable for the normal growth and development at least in mice, in stark contrast to the importance of *ALS2* in humans.

Our detailed investigation using immunohistochemical and electrophysiological techniques allowed us to detect some abnormalities in *Als2*-null mice that were not documented by Cai *et al.* (36). First, *Als2*-null mice develop an age-dependent, slowly progressive loss of cerebellar Purkinje cells. Secondly, these mice also develop late-life, subclinical

deficits of spinal motor neurons, evidenced by muscle fiber denervation followed by reinnervation and a reduction in numbers of ventral motor axons. Thirdly, *Als2*-null mice show increased astrogliosis and activation of inflammatory responses in brain and spinal cord. Lastly, in cultured *Als2*-null fibroblasts, trafficking and fusion of the internalized vesicles/membrane compartments are decreased. Collectively, these data document that the *Als2* null mutation causes age-dependent, subclinical dysfunction of motor system and intracellular membrane trafficking in mice.

It is notable that progressive loss of Purkinje cells is observed in *Als2*-null mice, implying that long-term absence of ALS2 expression in Purkinje cells and/or the surrounding environment disrupts normal homeostasis of these cells. In this study, we showed that ALS2 is expressed in the granular and Purkinje layers of the cerebellum in wild-type mice. We also found that ALS2 expression colocalizes with some, but not all calbindin immunopositive Purkinje cells, suggesting that ALS2 is expressed at least in subpopulations of Purkinje cells and surrounding cells. This is consistent with our previous studies that used *in situ* hybridization to document that *Als2* mRNA is strongly expressed in subpopulation of Purkinje cells (1). Devon *et al.* (31) demonstrated ALS2 expression in molecular and granular layers of the cerebellum, but not in Purkinje cells. Although it is conceivable that differences in ALS2 expression in Purkinje cells could reflect differences in our methodologies, the reason for this discrepancy remains elusive. In any case, a careful assessment of the cerebellar pathology, which has not been clinically implicated in ALS/MNDs, should be warranted not only in animal models but also in human ALS2/PLSJ/IAHSP cases.

MUNE is a highly sensitive method to estimate axon loss in diseases affecting the lower motor system (38). Notably, using this technique in conjunction with the assessment of ventral root, NMJ, and skeletal muscles, we detected abnormalities in the architecture of motor units in aged *Als2*-null mice. Our results demonstrating a decrease in MUNE and concurrent increase in SMUPs associated with abnormal NMJs, reduced ventral motor axons and muscle fiber-type grouping, all support the occurrence of fiber redistribution (denervation followed by reinnervation) and mild distal axonopathy in *Als2*-null mice. Recent studies have shown that abnormalities in the NMJ are an early finding in mice overexpressing mutant human SOD1 (39,40). Further, a decrease in the motor unit number in the distal hind limb was also evident before behavioral abnormalities appeared in the SOD1-transgenic mice (41), suggesting that a distal axonopathy is present in an early, pre-clinical phase in those ALS mice. Thus, the chronic, slowly progressing denervation and neurogenic atrophy observed in our *Als2*-null mice may also be an early and pre-clinical abnormality of the motor system dysfunction. Our observation of increased astrogliosis and activation of inflammatory responses without motor neuron death of spinal cord in *Als2*-null mice is consistent with this concept.

A corollary hypothesis suggested by these *in vivo* data is that loss of ALS2 is not rapidly detrimental but nonetheless mediates a long-term adverse effect on cellular physiology. Indeed, our cellular studies on the receptor-mediated endocytosis and trafficking of the internalized vesicles revealed that ALS2 is not required for either endocytosis or endosome trafficking. Nonetheless, a quantitative assessment of the fluorescence intensities of the EGF-labeled endosomes/vesicles demonstrated a significant decrease in its intensities at a 10 min point after the EGF internalization, implying that ALS2 might modulate an early phase of trafficking and fusion of the internalized vesicles and/or endosomal membrane compartments. The results support the concept that, at least in fibroblasts, ALS2 mediates modulatory functions on endosome dynamics via the activation of Rab5 (22,23,25). In addition to such endosome-related ALS2 function, a recent study has also revealed that loss of ALS2 predisposes neurons to oxidative stress (36), suggesting a possible neuroprotective role for ALS2. Further investigations on the effect of ALS2 loss in neuronal cells and a relationship between endosome dynamics and oxidative stress are in progress.

Given the subtle role of ALS2 in cellular physiology in mice, why do humans with *ALS2* mutations develop such severe phenotypes? Three explanations are proposed. First, the differences in the architecture of corticomotoneuronal systems may be critical. In rodents, it is generally believed that there is no direct synaptic connection between UMN and LMN in the spinal cord (42), which might be associated with the lack of overt motor phenotypes in *Als2*-null mice. Against this is the observation that, irrespective of their connectivity, neither UMN nor LMN in *Als2*-null mice showed overt degenerating phenotypes. A second possibility is the longer length of human motor axons. A recent pathological study of postmortem brain and spinal cord of patients with HSP has suggested that axonal loss in the corticospinal tract is length-dependent, but not size-selective (43). Further, recent evidence supports the view that axonal transport plays a crucial role in the maintenance of longer motor neurons in human (44,45) and mice (46–51). Because human motor axons are markedly longer than those in the mouse, it is conceivable that human motor neurons are more susceptible to defects in axonal trafficking caused by loss of ALS2. Thirdly, a specific compensatory mechanism or redundant gene expression could alleviate the disease phenotypes in mice. Alternatively, human may have a unique mechanism aggravating the disease when ALS2 is absent. We demonstrate here that there are differences in the expression pattern and sequence structure for short alternative splicing variants between human *ALS2* and mouse *Als2* genes. In addition, it has been reported that human and mouse ALS2CL proteins, novel ALS2 homologs, possess slightly different biochemical and enzymatic properties (33). Thus, these homologs and/or variants as well as yet unidentified factors including the ALS2-interacting proteins may explain the divergences of phenotypes in mice and humans devoid of ALS2.

In conclusion, our findings suggest that ALS2 is important in membrane trafficking, particularly in motor neurons and Purkinje cells. Our *Als2*-null mice might provide a unique resource to understand the interplay between membrane trafficking, endosomal dynamics and the long-term viability of large neurons such as Purkinje cells and spinal motor neurons. Ultimately, understanding these complex phenomena will provide insights into the molecular pathogenesis of MNDs arising from inactivating mutations in the *ALS2* gene.

MATERIALS AND METHODS

Genomic analysis of the mouse *Als2* gene and its expression

To characterize the potential variants for the mouse *Als2* gene, we conducted BLAST searches on the public databases. Cloning of the identified mouse short variants for the *Als2* gene was performed by a RT–PCR-based method. Expression and tissue distribution of the mouse *Als2* mRNA were characterized by northern blot analysis. Briefly, mouse adult tissue Multiple tissue northern (MTN) blot (BD Biosciences) was hybridized with the [^{32}P]dCTP-labeled mouse *Als2* or mouse glyceraldehydes 3-phosphate dehydrogenase (*Gapdh*) cDNA in PerfectHyb hybridization solution (Toyobo) at 68°C. Membranes were washed with 0.1 × SSC containing 1% sodium dodecyl sulfate (SDS) at 65°C and exposed to X-ray film (BioMax; Kodak).

Construction of the *Als2* targeting vector

A λFIXII 129SV/J genomic DNA library (Stratagene) was screened with the 5′ portion (1–595 nt) of the mouse *Als2* cDNA (GenBank accession no. AB053307). Eleven independent genomic clones covering ~29 kb genomic region containing exons 2–9 of the *Als2* gene were obtained and characterized by restriction enzyme mapping and DNA sequencing. A targeting vector was constructed by replacing a 39 bp fragment flanked by two *Bam*HI sites within the third exon of the *Als2* gene with the neomycin resistant gene (*neo*), as a positive selection marker, under the control of the phosphoglycerate kinase (PGK)-1 promoter. Further, the diphtheria toxin A (*DT-A*) gene, as a negative selection marker, was also used in this targeting vector. Briefly, the 5′-long *Spe*I/*Bam*HI fragment (9537 bp) containing a portion of intron 1, exon 2, entire intron 2 and the 5′ half of exon 3 was cloned into the *Spe*I/*Fba*I sites of the modified DT-A vector in which the *Not*I(mutated)–*Nru*I–*Spe*I–*Fba*I–TGA(stop codon)–*Cfr*9I–NotI linker was inserted at the original *Not*I site of the pMC1DTpA vector. The resulting 5′-fragment vector was digested with *Cfr*9I/*Not*I and linearized. Next, the 3′-short *Bam*HI/*Mlu*I fragment (1206 bp) containing 3′ half of exon 3 and intron 3 was cloned into the *Bgl*II/*Mlu*I sites of the modified neo-cassette vector in which the *Xho*I–*Bgl*II–*Mlu*I–*Not*I–*Xho*I(mutated) linker was introduced into the original *Xho*I site of the pKJ2(X^+) vector, and the resulting plasmid DNA was digested with *Cfr*9I/*Not*I to release the DNA fragment comprising the neo cassette connecting with the 3′-short fragment at the 3′ end. This *Cfr*9I/*Not*I fragment was ligated to the 5′-long linearized *Cfr*9I/*Not*I fragment and circularized. Finally, the generated plasmid DNA was digested with *Nru*I and linearized, generating the targeting vector for the third exon of mouse *Als2* gene, which resembled the mutation found in Tunisian ALS2 patients (1,2).

Generation of the *Als2* knockout mice

The linearized targeting vector was electroporated into E14.1 ES cells originated from 129/Ola strain, followed by the selection in G418 (52). Targeted clones were screened by PCR and Southern blot hybridization as described below. Among 507 G418-resistant E14.1 clones, 14 homologous recombinant clones (2.8%) were identified. After confirming the normal chromosome numbers and structure by karyotyping, six selected ES clones were subjected to the generation of chimera mice by the aggregation method using C57BL/6J blastocysts as the recipients (52). The resulting male chimeras were further mated with C57BL/6J female mice for germline transmission. Two ES clones (clones 17C6 and 21B5) gave germline chimeras, and we analyzed the knockout mice derived from clone 17C6. The heterozygous mice (F1 mice) were interbred to obtain wild-type, heterozygous and homozygous littermates (F2); the following generations (F3 and F4) were in a mixed 129Ola/C57BL6J (50%/50%) genetic background. Independently, the F1-heterozygous mice were also backcrossed to the C57BL/6J strain mice for four generations, and resulting heterozygous mutants (N4 mice) were interbred to obtain wild-type, heterozygous and homozygous littermates for the use of the primary cultured cells. The genotypes of the mice were determined by PCR and Southern blot analysis of genomic DNA obtained from the tails as below. Body weight of all animals was measured from 8 weeks of age and monthly (every 4 weeks) thereafter. Mice were allowed to freely access to food and water and housed at an ambient temperature of 23°C and at a 12 h light/dark cycle. All animal experiments were performed in accordance with the guidelines of the institutional committee on Animal Care and Use, and with the safety and ethical guidelines for gene manipulation experiments approved by the local institutional committee.

Polymerase chain reaction

Two pairs of primers allowing to specifically detect the mutant allele were designed as follows: neo-L1: 5′-ATCAGGATGA TCTGGACGAAGAGC-3′/mCR6out-R1: 5′-ACCTTCAAA GACTCAACTCAGAAGCCG-3′ (~2.4 kb) and neo-L2: 5′-TACCCGTGATATTGCTGAAGAGCTTG-3′/mCR6outR2: 5′-GTCCTGAGACAAAAGTCCTGCTATGCC-3′ (~2.2 kb). Approximately 100 ng of genomic DNA prepared from ES clones or tail tissues was subjected to the PCR amplification using KOD-PLUS-DNA polymerase (Toyobo) with 2 min of pre-denaturation at 94°C, followed by 10 cycles of 15 s at 94°C, 30 s at 62°C and 10 min at 68°C, and additional 35 cycles of 15 s at 94°C, 30 s at 62°C and 10 min with extending 10 s every cycle at 68°C. Another set of primers: mCR6ex03L1: 5′-AACCCTCCCACCATGTACCC-3′/mCR6 ex03R1: 5′-CCATTAGCATCGCTGTCCTG-3′ was designed to amplify the entire exon 3 and its flanking intronic sequences. Genomic DNA was amplified by LA *Taq* DNA polymerase (Takara) with a condition of 1 min of 94°C, followed by 35 cycles of 5 s at 98°C and 7 min at 68°C. The wild-type and mutant alleles gave rise to PCR-fragments of ~0.6 and ~2.2 kbp, respectively.

Southern blot analysis

Two independent probes, mCR6_probe1 (3′ external to the targeting vector) and mCR6_probe3 (5′ external to the targeting vector), were prepared by PCR amplification using the primer sets as follows: mCR6_probe1L: 5′-TTTCATCTCATATCAT

GGCGTATGG-3′/mCR6_probe1R: 5′-TCTCTGCTGAGTGA CAATGCCAG-3′ (product; 627 bp), and mCR6probe3-L: 5′-TTCTCGCTCTCTCTAAATAAATGTTG-3′/mCR6probe3-R: 5′-GTTTCCTTTTTGAAGTTTGAGTTATAATTTG-3′ (682 bp). In addition, the *neo* cassette was also utilized as a probe. Genomic DNA samples prepared from positive ES clones or tail tissues were digested with either *BglII* or *KpnI*, separated by electrophoresis, and blotted onto nylon membranes (Hybond; Amersham Biosciences). The *BglII* blot was hybridized with either mCR6_probe1, detecting an ~4 kb of the wild-type and/or an ~5.6 kb of the mutant alleles, or *neo* cassette, detecting only an ~5.6 kb of the mutant allele. The *KpnI* blot was hybridized with mCR6_probe3, allowing to detect an ~14.3 kb of the wild-type and/or an ~15.9 kb of the mutant alleles.

Antibodies

Three independent anti-ALS2 rabbit polyclonal antibodies, HPF1-680 (22), HPP1024 (22) and MPF1012–1651 (23), were used in this study. Anti-ALS2CL rabbit polyclonal antibody, CLHPF560–953, was newly generated by immunizing rabbits with the recombinant C-terminal fragment (amino acids 560–953) of human ALS2CL (33) and affinity-purified using an antigen-coupled sepharose column. Other antibodies used for western blot analysis were listed in Supplementary Material (see legend of Supplementary Material, Fig. S2). Antibodies used for immunohistochemical and immunocytochemical studies included rabbit polyclonal anti-MAP2 antibody (1:1000; CHEMICON), mouse monoclonal anti-βIII-tubulin (Tuji-1) antibody (Upstate), mouse monoclonal anti-GFAP antibody (1:500; CHEMICON), rat polyclonal anti-CD68 antibody (1:500; Serotec), rat polyclonal anti-CD11b antibody (1:500; Serotec), mouse monoclonal anti-SMI32 antibody (1:10 000; Sternberger Monoclonals) and mouse monoclonal anti-calbindin antibody (1:1000 for fluorescence, 1:5000 for histochemistry, Sigma).

Western blot analysis

Whole-tissue extracts were prepared from fresh mouse tissues by homogenizing in lysis buffer (25 mM Tris–HCl; pH 7.5, 5 mM $MgCl_2$, 50 mM NaCl, 1 mM dithiothreitol, 5% (w/v) sucrose, 1% (w/v) IGEPAL CA-630, protease inhibitor cocktail (Roche, Mannheim, Germany), 1 mM phenylmethylsulfonyl fluoride), denatured in Laemmli's SDS sample buffer, subjected to SDS–PAGE and transferred onto a polyvinylidene difluoride membrane (Bio-Rad). The membranes were blocked with 10% skim milk in TBST (20 mM Tris–HCl; pH 7.5, 150 mM NaCl, 0.1% Tween-20) overnight at 4°C and incubated with the indicated primary antibody for 2 h and with horseradish peroxidase-conjugated anti-rabbit or anti-mouse IgG sheep secondary antibody (Amersham Biosciences). Signals were visualized by the ECL PLUS system (Amersham Biosciences) and BioMax X-ray films (Kodak).

Rotarod tests

Motor performance, coordination and balance were evaluated with the rotarod apparatus (MK-660A; Muromachi Kikai) using an accelerating mode. Groups of age-matched F2 homozygous mutant ($Als2^{-/-}$, $n = 9$; four males and five females), heterozygous mutant ($Als2^{+/-}$, $n = 9$; four males and five females) and wild-type ($Als2^{+/+}$, $n = 9$; four males and five females) mice on a mixed 129Ola/C57BL6J genetic background were placed on the accelerating rod at a starting speed of 0 r.p.m., reaching a final speed of 80 r.p.m. in 1 min. Each mouse was given five trials per day during the light-cycle; the test was performed once a week starting from 8 to 81 weeks of age. The maximum speeds at which mice fall off from the rotarod were scored.

Histological and immunohistochemical analyses

The F2-homozygous mutant ($Als2^{-/-}$), heterozygous mutant ($Als2^{+/-}$) and wild-type ($Als2^{+/+}$) mice on a mixed 129Ola/C57BL6J genetic background (7–18 months of age) were used for histological and immunohistochemical studies. Animals were deeply anesthetized with 4% halothane and transcardially perfused with 4% paraformaldehyde (PFA) in 0.1 M phosphate buffer (PB) (pH 7.5). Brain, spinal cord and other organs were removed and post-fixed for at least 24 h in 4% PFA followed by cryoprotection in 30% sucrose in 0.1 M PB (pH 7.5) for 72 h and processed either for frozen tissue sectioning or for paraffin embedding. For fluorescent immunohistochemistry, 10 μm frozen sections were cut on a cryostat, and brain and spinal cord sections were incubated in phosphate-buffered saline (PBS, pH 7.6) with 3% normal goat serum and 0.3% Triton X-100 for 1 h at room temperature (Rtemp). For double immunostaining, sections were incubated with primary antibodies in PBS containing 0.01% Triton X-100 overnight at 4°C. Sections were incubated with CY3- or FITC-conjugated secondary antibodies (1:200 anti-mouse, Vector Laboratories; 1:300 anti-rabbit and anti-rat antibodies, Jackson ImmunoResearch Laboratories) for 3 h at Rtemp. TSA-amplification (Molecular probes) was used for fluorescent double labeling with anti-ALS2 and calbindin according to manufacturer's instructions. Formalin-fixed mouse brain samples were embedded in paraffin and sectioned at 7 mm thickness for immunohistochemistry for ALS2 using the affinity-purified anti-ALS2_RLD polyclonal antibody (HPF1-680) as described previously (22) with the following modifications: sections were incubated with 20 μg/ml trypsin (Zymed Laboratories) in PBS for 10 min at 37°C and washed in PBS prior to processing for normal immunohistochemistry. Sections were processed for DAB-immunostaining following a standard protocol using Vectorstain Elite ABC kit (Vector Laboratories) according to manufacturer's instructions and visualized using Nickel-enhanced DAB labeling as previously described (53). For identification of NMJs, fresh gastrocnemius muscle was harvested, post-fixed in 4% PFA for 24 h followed by 30% sucrose in 0.1 M PB for 24 h and sectioned longitudinally at 30 μm using a cryostat. Sections were incubated in PBS containing 0.2% Triton X-100, 5% normal goat serum, 2.5% bovine serum albumin (BSA) for 1 h at Rtemp followed by PBS containing αBTX conjugated to Alexa Fluor-594 (1:500; Molecular Probes) and anti-SMI32 (1:500) overnight at 4°C. Sections were washed and processed for fluorescent immunostaining using standard procedures. Controls for all immunostaining were performed sim-